

**Hydrodynamic inverse Faraday effect in a two-dimensional electron liquid**S. O. Potashin,<sup>1</sup> V. Yu. Kachorovskii <sup>1,2,3</sup> and M. S. Shur <sup>2</sup><sup>1</sup>*Ioffe Institute, 194021 St. Petersburg, Russia*<sup>2</sup>*Rensselaer Polytechnic Institute, Troy, New York 12180, USA*<sup>3</sup>*CENTERA Laboratories, Institute of High Pressure Physics, Polish Academy of Sciences, 01-142 Warsaw, Poland*

(Received 13 April 2020; revised 17 July 2020; accepted 20 July 2020; published 5 August 2020)

We show that a small conducting object, such as a nanosphere or a nanoring, embedded into or placed in the vicinity of a two-dimensional electron liquid (2DEL) and subjected to a circularly polarized electromagnetic radiation induces “twisted” plasmonic oscillations in the adjacent 2DEL. The oscillations are rectified due to the hydrodynamic nonlinearities leading to the helicity sensitive circular DC current and to a magnetic moment. This hydrodynamic inverse Faraday effect (HIFE) can be observed at room temperature in different materials. The HIFE is dramatically enhanced in a periodic array of the nanospheres forming a resonant plasmonic coupler. Such a coupler exposed to a circularly polarized wave converts the entire 2DEL into a vortex state. Hence, the twisted plasmonic modes support resonant plasmonic-enhanced gate-tunable optical magnetization. Due to the interference of the plasmonic and Drude contributions, the resonances have an asymmetric Fano-like shape. These resonances present a signature of the 2DEL properties not affected by contacts and interconnects and, therefore, providing the most accurate information about the 2DEL properties. In particular, the widths of the resonances encode direct information about the momentum relaxation time and viscosity of the 2DEL.

DOI: [10.1103/PhysRevB.102.085402](https://doi.org/10.1103/PhysRevB.102.085402)**I. INTRODUCTION**

Generation of stationary magnetic moments by circularly polarized radiation is commonly referred to as the inverse Faraday effect (IFE) predicted by Pitaevskii [1] and first observed by van der Ziel *et al.* [2]. Although this effect is usually studied in magnetic materials [3–5], it can also be observed in conventional semiconductor nanostructures such as quantum dots and nanorings [6–15]. In particular, it was recently predicted [14,15] that a circularly polarized radiation with the electric component  $\mathbf{E} = \mathbf{E}_\omega \exp(-i\omega t) + \text{c.c.}$  can excite a circular DC current in a nanoring, which, in turn, generates a magnetic moment:

$$\mathbf{M} \propto i \mathbf{E}_\omega \times \mathbf{E}_\omega^* \quad (1)$$

The proportionality coefficient in Eq. (1) is an odd function of frequency, so the effect is sensitive to the helicity of polarization. Remarkably, IFE is dramatically enhanced in the vicinity of plasmonic resonances [15]. Specifically, adjusting the plasmonic frequency in the nanoring to match the frequency of impinging radiation results in a much larger optically induced stationary magnetic field (up to 0.1 Gauss for typical parameters of a nanoring, see discussion in Ref. [15]). Hence, an array of nearly identical quantum rings should give rise to large optically controlled macroscopic magnetization. This opens a wide avenue for applications in tunable optoelectronics, in particular, in the terahertz (THz) range of frequencies.

The key feature of the plasmonic-enhanced IFE as compared to other plasma-wave-related effects is the absence of the symmetry limitations for conversion of incoming radiation into a DC signal. Indeed, in conventional plasmonic devices, such conversion requires an asymmetry of the system that determines the direction of the DC current. In two-dimensional

structures, the asymmetry can be created by the boundary conditions [16] or induced by ratchet effect (see Ref. [17] for review). The latter implies a special type of grating-gate couplers that could provide the required asymmetry. By contrast, IFE exists in fully symmetric rings [14,15] and the direction of the arising DC current is simply determined by the sign of the circular polarization. What is also important in view of possible applications for THz plasmonics is that the optically induced DC current remains finite even in the long-wavelength limit, when  $\mathbf{E}_\omega$  does not vary within the dimension of ring. Hence, the quantum nanorings and ring-based arrays can be used as effective helicity-driven sensors for THz radiation (see estimates and discussion in Ref. [15]).

In this paper, we discuss the possibility of observing similar effects in 2D systems. We consider the excitation of circular plasmonic modes (twisted plasmons) and circular DC currents in a two-dimensional electron liquid (2DEL). These modes are excited by a circularly polarized electromagnetic radiation impinging on the metallic or semiconducting nanosphere or nanoring embedded into or placed above the 2DEL and inducing rotating dipoles in these nanostructures [see Fig. 1(a)]. Rectification of the twisted plasmons due to hydrodynamic nonlinearities leads to a helicity-sensitive circular DC current and, consequently, to a magnetic moment, thus demonstrating the hydrodynamic inverse Faraday effect (HIFE). If the nanospheres form a 2D crystal [see Fig. 1(b)], only the plasmons with the wave vectors forming inverse crystal lattices are excited, so excitation spectrum becomes discrete. When the radiation frequency is close to any of the discrete plasmonic frequencies, the entire high-mobility 2DEL experiences a resonant circular plasmonic excitation. The rectification of these oscillations leads to a plasmonic-enhanced DC current which oscillates in space. The circular

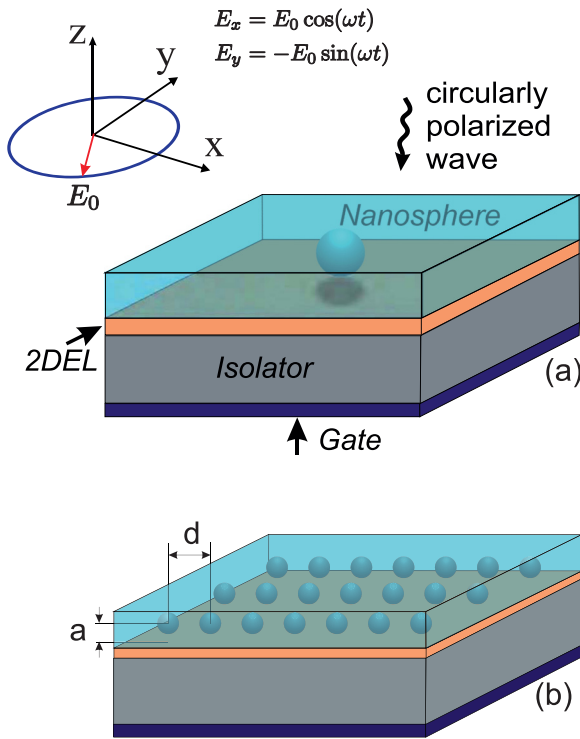


FIG. 1. Excitation of twisted plasmons in 2D electron liquid by a single nanosphere embedded into dielectric matrix and excited by circularly polarized radiation (a) or by an array of nanospheres forming a plasmonic coupler (b).

DC current and magnetic moment generated by this current show sharp HIFE resonances. Since the plasma wave frequency is tunable by the gate voltage and by an external magnetic field, such a system can be used for the optical tunable magnetization of 2D systems. The typical 2DEL twisted plasmon frequencies are in the THz range, and this coupling system could be used for tunable THz electronic components, including frequency multipliers, modulators, absorbers, and mixers. Another key application is in the contactless characterization and parameter extraction of the 2DEL.

Apart from these applications, there are some very interesting fundamental aspects of the HIFE related to hydrodynamic approach in plasmonics, the field which explores how electromagnetic fields can be confined over dimensions much smaller than the radiation wavelength [18–24]. The hydrodynamic approach to the description of the electronic systems and, in particular, the plasma wave excitation, has a long history which can be traced back to early work by Gurzhi [25] and by de Jong and Molenkamp [26], where hydrodynamic effects on the electron and phonon transport were discussed, and to the work by Dyakonov and Shur [16], which exploited the analogy between the “shallow water” hydrodynamics and that of the electron liquid in two-dimensional (2D) gated systems. Many other beautiful hydrodynamic phenomena such as choking of electron flow [27], nonlinear rectification of the plasma waves [28,29], and the formation of plasmonic shock waves [30] have been subsequently proposed. Possible applications of these phenomena to the plasma-wave electronics were intensively discussed (see Refs. [31,32]). More recent

interest to the hydrodynamic phenomena in low-dimensional transport and plasmonics is driven by the emergence of high-mobility nanostructures [33–41] and graphene [42–52] where the electron-electron collision-dominated transport regime can be reached.

Two issues that have been most actively discussed in recent years are the emergence of hydrodynamic regimes with nonzero vorticity (and their manifestation in the transport properties of the 2DEL) (see Refs. [40,48–52] and references therein), as well as possible methods for measuring the electron viscosity by using dynamic excitations of 2DEL [40] and by nonlocal resistance measurements [48–52].

Here we demonstrate that the electron flow with nonzero vorticity can be excited by circularly polarized radiation. Importantly, we find that such states appear even in an ideal 2DEL with zero viscosity. We also find that the main effect of viscosity is broadening of the plasmonic resonances in the structure shown in Fig. 1(b). The corresponding contribution to the resonance width is proportional to the kinematic viscosity and depends on the single geometrical factor—the distance  $d$  between nanospheres. This enables optical measurements of the electron liquid viscosity.

## II. MODEL

### A. Basic equations

In this paper, we consider circular (twisted) plasmon excitation through the periodic array of metal objects (or semiconducting objects with high conductivity), such as nanospheres or nanorings, embedded into or placed in the vicinity of the 2DEL by using insulating matrix transparent for the THz radiation. To begin, we consider the excitation by a single nanosphere [see Fig. 1(a)] and then generalize the results in the case of the grating plasmonic coupler consisting of a periodic array of nanospheres [see Fig. 1(b)].

Circularly polarized electromagnetic radiation induces a rotating dipole potential in the nanosphere. As a result, an inhomogeneous field is formed, which, in turn, acts on the 2DEL. We will find the DC response of the system. We assume that (i) electron-electron collisions prevail over scattering by phonons and impurities; (ii) the radiation wavelength is much larger than the radius of the nanosphere, so the electric field of radiation is uniform; and (iii) the system is gated. The first assumption allows us to use the hydrodynamic approximation.

The 2D electron liquid is described by the hydrodynamic equations for the dimensionless electron concentration  $n = (N - N_0)/N_0$  and velocity  $\mathbf{v}$ :

$$\frac{\partial n}{\partial t} + \text{div}[(1+n)\mathbf{v}] = 0, \quad (2)$$

$$\frac{\partial \mathbf{v}}{\partial t} + (\mathbf{v}\nabla)\mathbf{v} + \gamma\mathbf{v} + s^2\nabla n - \nu\Delta\mathbf{v} = \frac{e\mathbf{E}}{m}. \quad (3)$$

Here  $N_0$  is equilibrium concentration,  $s$  is the plasma wave velocity,  $\gamma$  is the rate of the momentum relaxation,  $\omega$  is the radiation frequency,  $m$  is the electron mass, and  $\nu$  is the kinematic viscosity. The field acting in the 2D plane,  $\mathbf{E} = \mathbf{E}_0(t) + \mathbf{E}_1(t, \mathbf{r})$ , is given by the sum of the homogeneous field of circularly

polarized incoming radiation,  $\mathbf{E}_0(t) = E_0(\cos \omega t, -\sin \omega t) = (E_0/2)(\mathbf{e}_x - i\mathbf{e}_y) \exp[-i\omega t] + \text{c.c.}$  and the dipole field

$$\mathbf{E}_1(\mathbf{r}, t) = -e\nabla \frac{\mathbf{rp}(t)}{(r^2 + a^2)^{3/2}}, \quad (4)$$

where  $\mathbf{p}(t) = p(\cos \omega t, -\sin \omega t)$  and  $ep = E_0R^3$  is the dipole moment of a metallic nanosphere with radius  $R$ . (Alternatively, one can use dielectric nanospheres with dielectric constant  $\epsilon_R$ . Then, the dipole moment becomes  $ep = E_0R^3(\epsilon_R + \epsilon)/(\epsilon_R + 2\epsilon)$ , where  $\epsilon$  is the dielectric constant of the transparent embedding matrix [53].) Here, we assume that internal plasmonic frequency of the nanospheres is very large as compared to characteristic frequencies of the problem, so spheres are fully polarized (corresponding estimates are given in Sec. VB). For a lattice of the nanospheres, one should replace  $\mathbf{E}_1(\mathbf{r}, t) \rightarrow \sum_i \mathbf{E}_1(\mathbf{r} - \mathbf{r}_i, t)$ , where summation is taken over the lattice nodes.

### B. Rectification of the optical signal

The incoming radiation leads to the oscillations of the concentration and velocity, which are rectified due to the nonlinearity of the hydrodynamic equations. The small signal solution of hydrodynamic equations Eqs. (2) and (3) can be found perturbatively by expansion over  $E_0$  up to the second order,

$$n \approx \delta n(t, \mathbf{r}) + \bar{n}(\mathbf{r}), \quad \mathbf{v} \approx \delta \mathbf{v}(t, \mathbf{r}) + \bar{\mathbf{v}}(\mathbf{r}),$$

where  $\delta n(t, \mathbf{r}) \propto E_0$  and  $\delta \mathbf{v}(t, \mathbf{r}) \propto E_0$  are oscillations of the concentration and velocity representing linear response and  $\bar{n}(\mathbf{r}) \propto E_0^2$  and  $\bar{\mathbf{v}}(\mathbf{r}) \propto E_0^2$  are time-independent corrections arising due to the rectification. We will see that the optically induced flow of the 2DEL with nonzero vorticity appears even in an ideal liquid with zero viscosity. Therefore, we will first put  $\nu = 0$  and discuss the viscosity-related effects at the end of the paper. One of our main findings is that a finite viscosity leads to a very simple contribution to the width of the plasmonic resonances and could be extracted from the measurements of the resonance width.

Due to the rectification, the impinging radiation induces both a DC current  $\mathbf{j}_{\text{DC}}$  and a static electric potential  $\phi_{\text{DC}}$ . To find the rectified corrections  $\bar{n}(\mathbf{r})$  and  $\bar{\mathbf{v}}(\mathbf{r})$  (squared-in- $E_0$ ), we average Eqs. (2) and (3) over time, thus arriving at the following set of the stationary equations:

$$\text{div } \bar{\mathbf{v}} = -\text{div } \mathbf{J}_1, \quad (5)$$

$$\gamma \bar{\mathbf{v}} + s^2 \nabla \bar{n} = \gamma \mathbf{J}_2, \quad (6)$$

with the rectified sources (we neglect terms of the order  $E_0^2$  oscillating at frequency  $2\omega$ . Such terms leads to negligible, on the order of  $E_0^4$ , corrections to the circular DC current):

$$\mathbf{J}_1 = \langle \delta n \delta \mathbf{v} \rangle_t, \quad \mathbf{J}_2 = -\frac{1}{\gamma} \langle (\delta \mathbf{v} \nabla) \delta \mathbf{v} \rangle_t. \quad (7)$$

To find total radiation-induced DC current,  $\mathbf{j}_{\text{DC}}$ , one should sum  $\bar{\mathbf{v}}$  and the rectified source  $\mathbf{J}_1$ . The radiation-induced potential,  $\phi_{\text{DC}}$  which creates static electric field  $E_{\text{DC}} = -\nabla \phi_{\text{DC}}$  is found from the condition  $e\nabla \phi_{\text{DC}}/m = s^2 \nabla \bar{n}$ . Thus, we have the following set of equations for  $\mathbf{j}_{\text{DC}}$  and  $\phi_{\text{DC}}$ :

$$\mathbf{j}_{\text{DC}}(\mathbf{r}) = N_0[\bar{\mathbf{v}}(\mathbf{r}) + \mathbf{J}_1(\mathbf{r})], \quad (8)$$

$$e\phi_{\text{DC}}(\mathbf{r}) = ms^2 \bar{n}(\mathbf{r}). \quad (9)$$

Hence, the key steps of the calculations are as follows. One should first linearize hydrodynamic Eqs. (2) and (3) and find the linear response. The next step is to substitute thus found  $\delta n$  and  $\delta \mathbf{v}$  into the expressions for the nonlinear sources given by Eqs. (7), perform the time averaging, and find  $\mathbf{J}_{1,2}$ . Then, one should calculate  $\bar{n}$  and  $\bar{\mathbf{v}}$  by solving Eqs. (5) and (6) and, finally, find  $\mathbf{j}_{\text{DC}}$  and  $\phi_{\text{DC}}$  from Eqs. (8) and (9).

### III. LINEAR RESPONSE: DRUDE AND PLASMONIC CONTRIBUTIONS

Since the electric field entering the right-hand side (r.h.s.) of Eq. (3) has both homogeneous and inhomogeneous contributions, one can present the velocity oscillations as the sum of the homogeneous Drude excitation and inhomogeneous dipole-induced plasmonic term, while

$$\delta \mathbf{v} = \delta \mathbf{v}^{\text{D}} + \delta \mathbf{v}^{\text{P}}. \quad (10)$$

Corrections to the concentration appear only due to the inhomogeneous perturbation, so  $\delta n = \delta n^{\text{P}}$ . As we demonstrate below, the presence of these two types of velocity excitations leads to interference effects and, as a consequence, to the Fano-like asymmetry of the resonances.

Linearizing Eqs. (2) and (3) and writing  $\delta n = \delta n_{\omega}(\mathbf{r})e^{-i\omega t} + \text{c.c.}$ ,  $\delta \mathbf{v} = \delta \mathbf{v}_{\omega}(\mathbf{r})e^{-i\omega t} + \text{c.c.}$ , after simple calculations (see Appendix A), we get

$$\delta n_{\omega}(\mathbf{r}) = \Delta Z(\mathbf{r}), \quad (11)$$

$$\delta \mathbf{v}_{\omega}(\mathbf{r}) = \underbrace{i\omega \nabla Z(\mathbf{r})}_{\delta \mathbf{v}_{\omega}^{\text{D}}} + \underbrace{\frac{eE_0(\mathbf{e}_x - i\mathbf{e}_y)}{2m(\gamma - i\omega)}}_{\delta \mathbf{v}_{\omega}^{\text{P}}}, \quad (12)$$

where, for the case of a single nanosphere,

$$Z(\mathbf{r}) = -i2\pi l^2 \int \frac{d^2q}{(2\pi)^2} \frac{e^{i\mathbf{q}\mathbf{r}} e^{-i\varphi_{\mathbf{q}}} e^{-q a}}{q^2 - k^2}. \quad (13)$$

Here  $e^{-i\varphi_{\mathbf{q}}} = (q_x - iq_y)/q$ ,

$$l^2 = \frac{e^2 p}{2ms^2} \quad (14)$$

and

$$k = \frac{\sqrt{\omega(\omega + i\gamma)}}{s} = k_0 + iQ. \quad (15)$$

The real and imaginary parts of  $k$ , respectively,  $k_0$  and  $Q$ , have a physical meaning of the wave vector and the spatial decrement of the optically excited plasma wave. In what follows, we assume  $\gamma \ll \omega$ . Hence,  $k \approx (\omega + i\gamma/2)/s$ , and, consequently,  $k_0 \approx \omega/s$ ,  $Q \approx \gamma/2s$ . As seen, the spatial decrement of the wave is small:

$$Q \ll k_0. \quad (16)$$

For the case of square dipole lattice with the lattice constant  $d$ , Eq. (13) is slightly modified by the replacement (see Appendix E),

$$\int \frac{d^2q}{(2\pi)^2} \rightarrow \frac{1}{d^2} \sum_{\mathbf{q}}$$

where wave vector  $\mathbf{q}$  runs over the inverse lattice vectors:

$$\mathbf{q}_{nm} = \frac{2\pi}{d}(n\mathbf{e}_x + m\mathbf{e}_y). \quad (17)$$

Since velocity is given by the sum of two terms [see Eq. (10)], one can split both of the rectified sources  $\mathbf{J}_{1,2}$  into two contributions—the plasmonic contribution and the mixed (plasmonic+Drude) contribution:

$$\mathbf{J}_i = \mathbf{J}_i^{\text{P}} + \mathbf{J}_i^{\text{M}} (i = 1, 2),$$

where

$$\begin{aligned} \mathbf{J}_1^{\text{P}} &= \langle \delta n^{\text{P}} \delta \mathbf{v}^{\text{P}} \rangle_t, & \mathbf{J}_2^{\text{P}} &= -\frac{\langle (\delta \mathbf{v}^{\text{P}} \nabla) \delta \mathbf{v}^{\text{P}} \rangle_t}{\gamma}, \\ \mathbf{J}_1^{\text{M}} &= \langle \delta n^{\text{P}} \delta \mathbf{v}^{\text{D}} \rangle_t, & \mathbf{J}_2^{\text{M}} &= -\frac{\langle (\delta \mathbf{v}^{\text{D}} \nabla) \delta \mathbf{v}^{\text{P}} \rangle_t}{\gamma}, \end{aligned} \quad (18)$$

Equations Eq. (13) and (18) allow us to clarify basic physics issues in more detail. First, as seen, the integral on the r.h.s. of Eq. (13) contains a pole in the denominator, which reflects the plasmonic resonance occurring when  $\omega$  is equal to the frequency of the plasma wave with the wave vector  $q$ . However, the pole is smeared out due to the integration over  $\mathbf{q}$ . The situation is different for a dipole lattice when the integration should be replaced with summation. For small  $\gamma$ , the contributions of the different terms in the sum are well separated and can give sharp plasmonic resonances. The resonance condition,

$$\omega = \omega_{nm} = (2\pi s/d)\sqrt{n^2 + m^2}, \quad (19)$$

is satisfied for several pairs  $(n, m)$ . For example, the fundamental plasmonic resonance with the frequency

$$\omega_0 = \frac{2\pi s}{d} \quad (20)$$

corresponds to the sum over four pairs  $(1, 0)$ ,  $(-1, 0)$ ,  $(0, 1)$ , and  $(0, -1)$ , yielding

$$Z_0(\mathbf{r}) \propto \frac{1}{\omega_0^2 - \omega^2 - i\omega\gamma}, \quad (21)$$

with the frequency-independent coefficient of proportionality. Then, rectified DC currents have the resonance dependence  $\mathbf{J}_i^{\text{P}} \propto |Z(\mathbf{r})|^2$ ,  $\mathbf{J}_i^{\text{M}} \propto Z(\mathbf{r})$ . As a result, in the vicinity of the resonance, the expression for the circular DC current can be approximately presented as follows:

$$\mathbf{j}_{\text{DC}} \approx \frac{\boldsymbol{\pi}(\mathbf{r})}{\Omega^2 + \Gamma^2/4} + \left[ \frac{\boldsymbol{\mu}(\mathbf{r})}{\Omega + i\Gamma/2} + \text{c.c.} \right], \quad (22)$$

where

$$\Omega = \frac{\omega - \omega_0}{\omega_0}, \quad \Gamma = \frac{\gamma}{\omega_0}, \quad (23)$$

are, respectively, the dimensionless detuning and damping of the fundamental resonance, while the terms proportional to vectors  $\boldsymbol{\pi}(\mathbf{r})$  and  $\boldsymbol{\mu}(\mathbf{r})$  represent the plasmonic and mixed contributions, respectively [exact expressions for these coefficients will be given below, see Eqs. (40), and (41)]. Due to the interference of these terms, the resonance in  $\mathbf{j}_{\text{DC}}$  and  $\phi_{\text{DC}}$  has an asymmetric Fano-like shape. Interestingly enough, the degree of asymmetry depends on the coordinate  $\mathbf{r}$ .

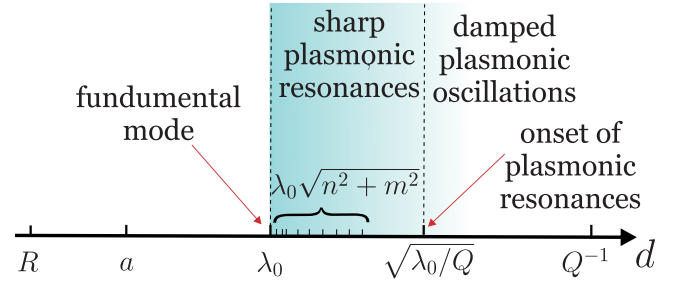


FIG. 2. Different scales of the problem. We predict sharp plasmonic resonances for  $\lambda_0 < d < \sqrt{\lambda_0/Q}$ .

Different scales of the problem are illustrated in Fig. 2. The smallest scale is the size of the sphere,  $R$ , which is on the order or smaller than the distance from spheres to the plane of 2D gas,  $R \lesssim a$ . We assume that the wavelength of the plasma excitations,  $\lambda_0 = 2\pi/k_0$ , is much larger than  $a$  but smaller than the plasma wave damping length:  $a \ll \lambda_0 \ll Q^{-1}$ . For  $d \gg Q^{-1}$ , the spheres are fully independent and it is sufficient to calculate the response of a single sphere. With decreasing  $d$ , the spheres begin to influence each other. One can easily estimate characteristic  $d$  corresponding to the onset of plasmonic resonances. To this end, we estimate the volume in the momentum space corresponding to a plasmonic resonance as  $k_0 Q$ . When this volume becomes smaller than the volume of the unit cell of the inverse lattice,  $k_0 Q \ll (2\pi/d)^2$ , the resonances cease to overlap. The fundamental mode corresponds to a smaller intersphere distance:  $d = \lambda_0$ . The total number of well-resolved resonances that can be observed is proportional to  $k_0/Q = \omega/\gamma$  and is thus determined by the quality factor. It is worth noting that sharp resonances exist in the finite range of  $d$ :  $\lambda_0 \lesssim d \lesssim \sqrt{\lambda_0/Q}$ .

An important comment is related to the radiation-induced vorticity of the 2DEL. On the formal level, function  $Z(\mathbf{r})$  is a Green's function of hydrodynamic equations describing the plasmonic excitation caused by a pointlike rotating dipole. Due to this rotation, an angular momentum  $\pm 1$  is transferred to the liquid with the sign determined by the sign of the helicity. The information about this moment is encoded in the phase factor  $\exp[-i\varphi_{\mathbf{q}}]$  in Eq. (13). This means that the plasma waves circulate around the nanospheres and that the direction of circulation changes with changing the sign of the radiation polarization. We call such excitations twisted plasmons. The rectification of these plasmons leads to DC current with nonzero vorticity, which is also determined by the helicity sign.

#### IV. CIRCULAR DC CURRENT INDUCED BY A SINGLE DIPOLE

Performing integration over  $\varphi_{\mathbf{q}}$  in Eq. (13), we get

$$Z(\mathbf{r}) = l^2(x - iy)f(r), \quad (24)$$

where function  $f$  depends only on  $r = |\mathbf{r}|$ . The analytical expressions for  $f$  and its asymptotes are presented in the Appendix A together with expression of  $\delta n_\omega$  and  $\delta v_\omega$  in terms of  $f$ . It is convenient to present  $\mathbf{J}_i$  as follows:

$$\mathbf{J}_i = R_i \mathbf{e}_r + \Phi_i \mathbf{e}_\phi, \quad (25)$$

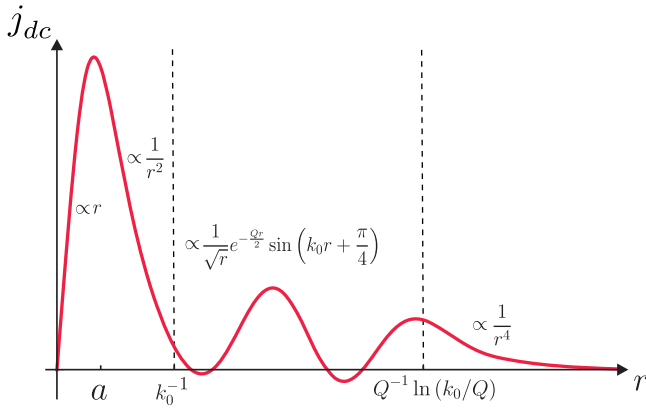


FIG. 3. Dependence of the circular current density,  $j_{DC}$ , created in 2D liquid by a rotating dipole moment of a single nanosphere. Main contribution to this current comes from mixed term [see Eq. (28)].

where  $\mathbf{e}_r = \mathbf{r}/r$ ,  $\mathbf{e}_\varphi = \mathbf{e}_z \times \mathbf{e}_r$  and functions  $R_i = R_i^P + R_i^M$ , and  $\Phi_i = \Phi_i^P + \Phi_i^M$ , depend only on  $r = |\mathbf{r}|$  and contain both plasmonic and mixed contributions. Here, vector  $\mathbf{r}$  is counted from the center of nanosphere [see Fig. 1(a)].

Provided that  $R_i$  and  $\Phi_i$  are known, the solution of Eqs. (5) and (6) can be found by expanding  $\bar{\mathbf{v}}$  over  $\mathbf{e}_r$  and  $\mathbf{e}_\varphi$  and assuming  $\bar{n} = \bar{n}(r)$ . We find for the total circular radiation-induced DC current,  $\mathbf{j}_{DC} = j_{DC}\mathbf{e}_\varphi$  and the radial electric field,  $E_{DC} = E_{DC}\mathbf{e}_r$ :

$$j_{DC} = N_0(\Phi_1 + \Phi_2), \quad (26)$$

$$\frac{eE_{DC}}{m} = \gamma(R_1 + R_2) \quad (27)$$

Expressions for plasmonic and mixed contributions,  $R_i^P$ ,  $\Phi_i^P$ , and  $R_i^M$ ,  $\Phi_i^M$ , are presented in Appendixes B and C, respectively, as well as expressions for asymptotical behavior of  $j_{DC}$  [see Eq. (D1)] and  $E_{DC}$  [see Eq. (D2)], accounting for both plasmonic and mixed contributions. As seen, for the most realistic case ( $R \ll a \ll k_0^{-1} \ll Q^{-1}$ ), the mixed contribution dominates. Neglecting plasmonic contribution, we find that

$$j_{DC} \approx -j_* \begin{cases} C\left(\frac{r}{a}\right), & r \ll 1/k_0 \\ \frac{\sqrt{2\pi}k_0^{3/2}a^2}{\sqrt{r}} e^{-Qr/2} \sin(k_0r + \pi/4), & 1/k_0 \ll r \ll \frac{\ln[k_0/Q]}{Q} \\ \frac{6a^2}{k_0^2 r^2}, & \frac{\ln[k_0/Q]}{Q} \ll r, \end{cases} \quad (28)$$

where

$$j_* = \frac{\omega l^4 N_0}{k_0^2 R^3 a^2}, \quad (29)$$

and  $C(x)$  is given by Eq. (D4). Schematic dependence of  $j_{DC}$  on  $r$  is shown in Fig. 3. The static optically induced field is linked to the DC circular current by a simple relation:

$$j_{DC} = -\frac{eE_{DC}N_0}{m\omega}. \quad (30)$$

### A. Dipole lattice

For a lattice of dipoles, we write the Fourier components of the nonlinear sources  $\mathbf{J}_1$  and  $\mathbf{J}_2$  as follows:

$$\mathbf{J}_{i\mathbf{q}\omega} = R_{i\mathbf{q}}\mathbf{n}_{\mathbf{q}}^\parallel + \Phi_{i\mathbf{q}}\mathbf{n}_{\mathbf{q}}^\perp, \quad i = (1, 2), \quad (31)$$

where  $\mathbf{n}_{\mathbf{q}}^\parallel = \mathbf{q}/q$  and  $\mathbf{n}_{\mathbf{q}}^\perp = \mathbf{e}_z \times \mathbf{q}/q$ . The Fourier transform of Eqs. (5) and (6) yields expressions similar to Eqs. (26) and Eq. (27):

$$\mathbf{j}_{\mathbf{q}}^{DC} = N_0(\Phi_{1\mathbf{q}} + \Phi_{2\mathbf{q}})\mathbf{n}_{\mathbf{q}}^\perp, \quad (32)$$

$$\frac{e\mathbf{E}_{\mathbf{q}}^{DC}}{m} = \gamma(R_{1\mathbf{q}} + R_{2\mathbf{q}})\mathbf{n}_{\mathbf{q}}^\parallel. \quad (33)$$

The Fourier components of the DC current and static field can be presented as sums over the plasmonic and mixed contributions:  $R_{i\mathbf{q}} = R_{i\mathbf{q}}^P + R_{i\mathbf{q}}^M$ ,  $\Phi_{i\mathbf{q}} = \Phi_{i\mathbf{q}}^P + \Phi_{i\mathbf{q}}^M$ .

We consider the simplest case of a square lattice with the lattice constant  $d$ . In this case, all the integrals over  $\mathbf{q}$  should be replaced with the sums over the vectors of the inverse lattice [see Eq. (17)] and function  $Z(\mathbf{r})$  becomes

$$Z(\mathbf{r}) = -\frac{i2\pi l^2}{d^2} \sum_{\mathbf{q}} \frac{e^{i\mathbf{q}\mathbf{r}}}{q^2 - k^2} e^{-i\varphi_{\mathbf{q}}} e^{-q a}. \quad (34)$$

Using this equation, we find

$$\delta n_\omega = \frac{2i\pi l^2}{d^2} \sum_{\mathbf{q}} \frac{e^{i\mathbf{q}\mathbf{r}} e^{-i\varphi_{\mathbf{q}}} q^2 e^{-q a}}{q^2 - k^2}, \quad (35)$$

$$\delta \mathbf{v}_\omega = \frac{2i\pi l^2}{d^2} \sum_{\mathbf{q}} \frac{e^{i\mathbf{q}\mathbf{r}} e^{-i\varphi_{\mathbf{q}}} \omega \mathbf{q} e^{-q a}}{q^2 - k^2} + \frac{eE_0(\mathbf{e}_x - i\mathbf{e}_y)}{2m(\gamma - i\omega)}. \quad (36)$$

The rectified currents  $\mathbf{J}_i^{P,M}$  can be calculated using Eqs. (18), (35), and (36). Corresponding analytical expressions are given in Appendix E. Resulting equations for  $\mathbf{j}_{DC}$  and  $\mathbf{E}_{DC}$  are given, respectively, by Eqs. (E9) and (E10).

In Fig. 4, we plotted the  $x$  component of the DC current in units of

$$j_0 = N_0 \frac{4\pi^2 l^4 s}{d^4},$$

in a certain point in the plane (we used  $x = y = d/8$ ) as a function of the radiation frequency for different damping rates (picture for the  $y$  component of the current looks analogous). As seen, with decreasing the  $\gamma$ , sharp resonances appear on the top of the smooth dependence. Due to the interference of the plasmonic and mixed contributions, the resonances have an asymmetric shape. The degree of asymmetry is smaller for small  $\gamma$  because the symmetric plasmonic contribution dominates at  $\gamma \rightarrow 0$ . Figure 5 illustrates the asymmetry of the peaks for fundamental mode. To demonstrate vorticity of the current, we also plotted the calculated current vector density in Fig. 6.

### B. Excitation of the fundamental mode

The smallest resonant frequency,  $\omega_0$ , is given by Eq. (20). This frequency corresponds to the contribution of four terms,

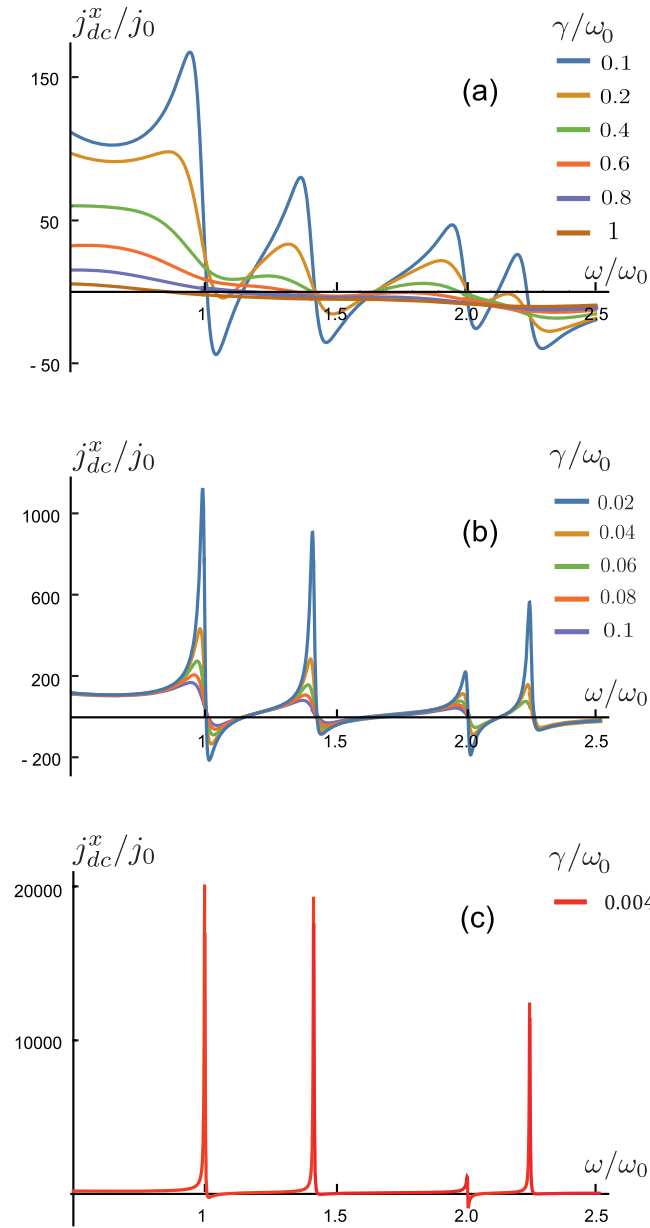


FIG. 4. Frequency dependence of  $x$ - component of the current density for  $x = y = d/8$ ,  $R = a/2$ ,  $d = 5a$ : onset of plasmonic resonances at large  $\gamma$ ; (a) strongly asymmetric resonances at intermediate values of  $\gamma$ , (b) weakly asymmetric resonances at very small  $\gamma$  (c).

with

$$(n, m) = (1, 0), (0, 1), (-1, 0), (0, -1). \quad (37)$$

For all these terms, we have  $q = q_0 = 2\pi/d$ . The frequency of the next resonance is given by  $\sqrt{2}\omega_0$ . It corresponds to the other four terms with  $(n, m) = (\pm 1, \pm 1)$ . For sufficiently high-quality factors,

$$\omega_0/\gamma \gg 1,$$

these two resonances are well separated. Hence, for  $\omega$  close to  $\omega_0$ , only four terms corresponding to Eq. (37) contribute to the sum over  $\mathbf{q}_{nm}$ , while terms with other  $n$  and  $m$  can be neglected (this corresponds to the resonance approximation).

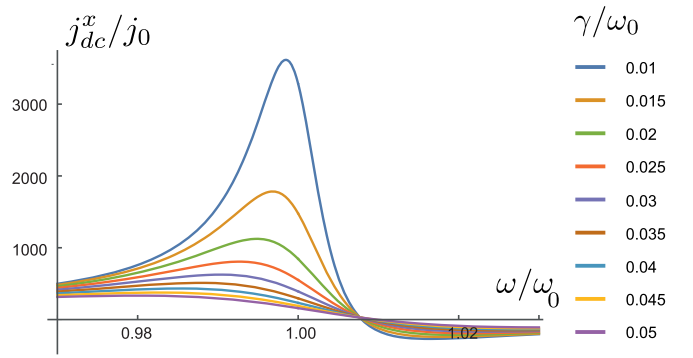


FIG. 5. Fundamental plasmonic peak in  $x$  component of DC current for  $x = y = d/8$ ,  $R = a/2$ ,  $d = 5a$  and different values of  $\gamma$ . The asymmetry of the peak decreases with decreasing of  $\gamma$ .

Within the resonance approximation, the concentration and velocity are given by

$$\delta n_\omega = \frac{4\pi l^2}{d^2} \frac{q_0^2 e^{-q_0 a} [i \sin(q_0 y) - \sin(q_0 x)]}{q_0^2 - k^2}, \quad (38)$$

$$\delta \mathbf{v}_\omega = \frac{4\pi l^2}{d^2} \frac{\omega q_0 e^{-q_0 a} [i \mathbf{e}_x \cos(q_0 x) + \mathbf{e}_y \cos(q_0 y)]}{q_0^2 - k^2} + \frac{e E_0 (\mathbf{e}_x - i \mathbf{e}_y)}{2m(\gamma - i\omega)}. \quad (39)$$

Using the equations given in Appendix F, we find that the circular current can be presented in the form of Eq. (22), with

$$\boldsymbol{\pi}(\mathbf{r}) = \pi_0 [\sin(q_0 y) \cos(q_0 x) \mathbf{e}_x - \sin(q_0 x) \cos(q_0 y) \mathbf{e}_y], \quad (40)$$

$$\boldsymbol{\mu}(\mathbf{r}) = \mu_0 [\sin(q_0 y) \mathbf{e}_x - \sin(q_0 x) \mathbf{e}_y], \quad (41)$$

where

$$\pi_0 = \frac{8\pi^2 N_0 s l^4}{d^4} e^{-2q_0 a}, \quad \mu_0 = \frac{N_0 s l^4}{d R^3} e^{-q_0 a}. \quad (42)$$

As seen,  $\text{div} \boldsymbol{\pi} = \text{div} \boldsymbol{\mu} = 0$ , so  $\mathbf{j}_{DC}$  is purely circular current,  $\text{div} \mathbf{j}_{DC} = 0$ , with nonzero vorticity:

$$\nabla \times \mathbf{j}_{DC} = -\mathbf{e}_z \frac{2q_0}{\Omega^2 + \Gamma^2/4} \{ \pi_0 \cos(q_0 x) \cos(q_0 y) + \mu_0 \Omega [\cos(q_0 x) + \cos(q_0 y)] \}. \quad (43)$$

Two interfering contributions, plasmonic and mixed, have different frequency dependencies in the vicinity of the resonance, symmetric and asymmetric ones, respectively. Interestingly, the degree of asymmetry depends on coordinate. For example, at the line  $\cos(q_0 x) + \cos(q_0 y) = 0$ , the vorticity is a symmetric function of  $\Omega$ , while for  $\cos(q_0 x) = 0$  or  $\cos(q_0 y) = 0$ , the vorticity is described by an asymmetric mixed term. The vector density plot of the rectified current  $\mathbf{j}_{DC}$  is plotted in Fig. 6 for different values of parameter,

$$\alpha = \frac{2\Omega \mu_0}{\pi_0} = \frac{d^3 \Omega}{4\pi^2 R^3} e^{q_0 a}, \quad (44)$$

which depends on the dimensionless deviation from the resonance,  $\Omega$ . Hence, changing radiation frequency, one can qualitatively change the spatial distribution of the DC current. To understand this dependence better, we rewrite Eq. (22) as

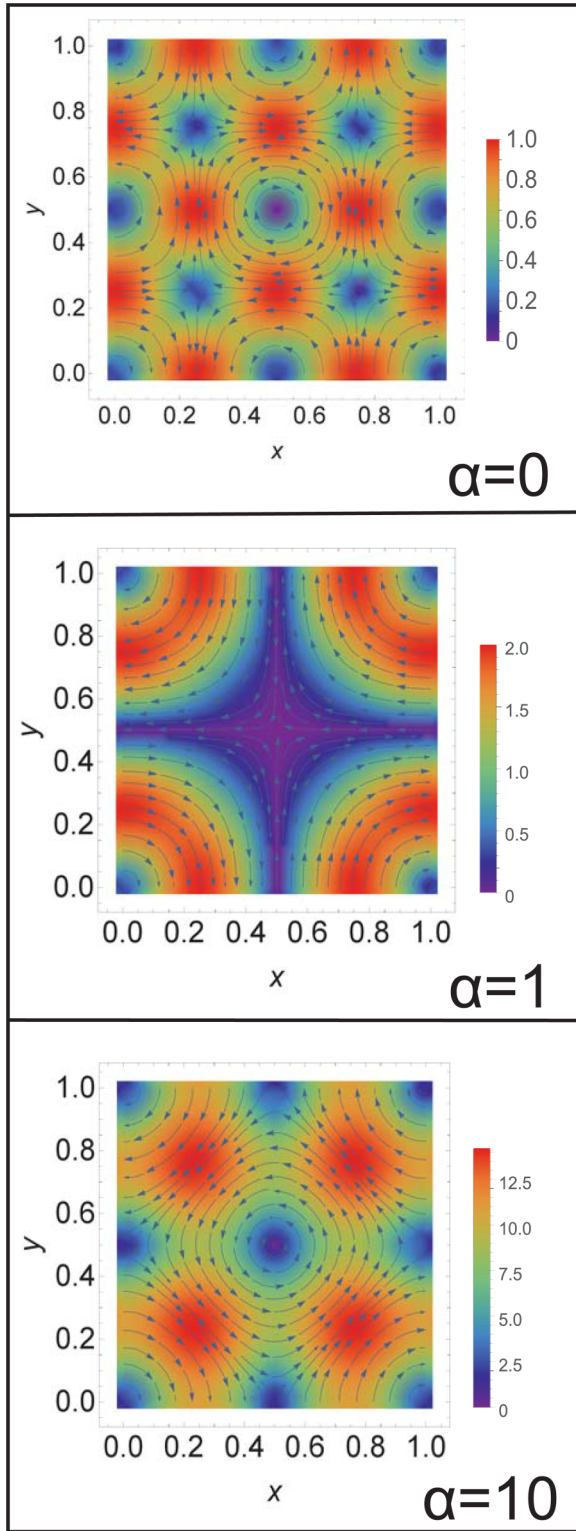


FIG. 6. Vector density plot of the rectified current density  $\mathbf{j}_{\text{DC}}$  for different values of parameter  $\alpha = 2\Omega\mu_0/\pi_0$  (here,  $x$  and  $y$  are measured in units of  $d$ ).

follows:

$$\frac{\mathbf{j}_{\text{DC}}}{j_0} = \frac{2e^{-2q_0\alpha}}{\Omega^2 + (\Gamma/2)^2} \{ \mathbf{e}_x \sin(q_0 y) [\alpha + \cos(q_0 x)] - \mathbf{e}_y \sin(q_0 x) [\alpha + \cos(q_0 y)] \}. \quad (45)$$

As seen, the key parameter which determines the current distribution is  $\alpha$ . Below, we will analyze the vector structure of this equation. For brevity, we skip common coefficient  $2j_0 e^{-2q_0\alpha} / [\Omega^2 + (\Gamma/2)^2]$  in the expressions for current.

For  $\alpha \ll 1$ , we get

$$\mathbf{j}_{\text{DC}} \propto \mathbf{e}_x \sin(q_0 y) \cos(q_0 x) - \mathbf{e}_y \sin(q_0 x) \cos(q_0 y)$$

$$j_{\text{DC}}^2 \propto \frac{1 - \cos(2q_0 x) \cos(2q_0 y)}{2}.$$

From these equations, we find that the current reaches its maximum absolute value at points  $\mathbf{r}_{nm}^I = (x_n^I, y_m^I) = (d/2)(n + 1/2, m)$  and  $\mathbf{r}_{nm}^{II} = (x_n^{II}, y_m^{II}) = (d/2)(n, m + 1/2)$  (here and below,  $n$  and  $m$  are integer numbers). These points correspond to centers of red circles in Fig. 6(a). From Eq. (45), we find values of currents,  $\mathbf{j}_{\text{DC}}^I$  and  $\mathbf{j}_{\text{DC}}^{II}$ , exactly at  $\mathbf{r}^I$  and  $\mathbf{r}^{II}$ , respectively, and their variations,  $\delta\mathbf{j}_{\text{DC}}^I$ ,  $\delta\mathbf{j}_{\text{DC}}^{II}$ , in the vicinity of these points

$$\mathbf{j}_{\text{DC}}^I \propto -\mathbf{e}_y (-1)^{n+m},$$

$$\delta\mathbf{j}_{\text{DC}}^I \propto (-1)^{n+m} q_0^2 \left( \mathbf{e}_y \frac{\delta x^2 + \delta y^2}{2} - \mathbf{e}_x \delta x \delta y \right),$$

$$\mathbf{j}_{\text{DC}}^{II} \propto \mathbf{e}_x (-1)^{n+m},$$

$$\delta\mathbf{j}_{\text{DC}}^{II} \propto (-1)^{n+m} q_0^2 \left( -\mathbf{e}_x \frac{\delta x^2 + \delta y^2}{2} + \mathbf{e}_y \delta x \delta y \right).$$

Here,  $\delta\mathbf{r} = (\delta x, \delta y)$  is a small deviation of  $\mathbf{r}$  from point  $\mathbf{r}^I$  or  $\mathbf{r}^{II}$  ( $q_0 \delta r \ll 1$ ). Analyzing these equations and Fig. 6(a), we see that there are eight current maxima (per unit cell of arising periodic structure) with different current behavior. Here  $\delta x$  and  $\delta y$  are counted from  $\mathbf{r}^I$  or  $\mathbf{r}^{II}$ . For  $\alpha \gg 1$ , we find that the current is given by

$$\mathbf{j}_{\text{DC}} \propto \alpha [\mathbf{e}_x \sin(q_0 y) + \mathbf{e}_y \sin(q_0 x)],$$

$$j_{\text{DC}}^2 \propto \alpha^2 [\sin^2(q_0 y) + \sin^2(q_0 x)].$$

We see that dependencies on  $x$  and  $y$  fully decouple. The current is maximal at points  $(x_n, y_m) = (d/2)(n + 1/2, m + 1/2)$ , corresponding to centers of the red circles in Fig. 6(c). Close to these points, we get

$$\mathbf{j}_{\text{DC}} \propto (-1)^m \alpha \mathbf{e}_x \left( 1 - \frac{q_0^2 \delta y^2}{2} \right) + (-1)^n \alpha \mathbf{e}_y \left( 1 - \frac{q_0^2 \delta x^2}{2} \right). \quad (46)$$

Hence, in this case, there are four maxima with different current behaviors per unit cell of the periodic current structure.

The vector density plots for  $\alpha \ll 1$  and  $\alpha \gg 1$  are essentially different. The transition between these plots happens at  $\alpha \sim 1$ . Let us consider, for example, the quadrant of the unit cell of the periodic structure of the current, corresponding to  $0 < x < d/2$  and  $0 < y < d/2$  (behavior in the remaining three quadrants can be considered analogously). For  $\alpha = 0$ ,  $j_{\text{DC}}^2$  has four maxima of equal heights at points  $\mathbf{r}_{00}^{II}$ ,  $\mathbf{r}_{00}^I$ ,  $\mathbf{r}_{01}^I$ , and  $\mathbf{r}_{10}^{II}$  [see Fig. 6(a)]. With increasing  $\alpha$ , the first two maxima increase by a factor  $(1 + \alpha)^2$ , while the second two decrease by a factor  $(1 - \alpha)^2$ . Also, for  $\alpha < \sqrt{8/3}$  there

is a saddle point in this quadrant at

$$x = y = \frac{d}{2\pi} \arccos\left(\frac{2}{\alpha + \sqrt{\alpha^2 + 8}}\right). \quad (47)$$

The squared current at the saddle point is

$$j_{\text{DC}}^2 \propto \frac{4(2 + a(a + \sqrt{8 + a^2}))^3}{(a + \sqrt{8 + a^2})^4}. \quad (48)$$

At  $\alpha > \sqrt{8/3}$ , the saddle point transforms to a maximum and the amplitude of this maximum becomes higher than for the maxima at points  $\mathbf{r}_{00}^{\text{II}}$ ,  $\mathbf{r}_{00}^{\text{I}}$ . With further increase of  $\alpha$ , the new maximum moves to the point  $(x, y) = (d/4, d/4)$ , and stops at this position for  $\alpha \rightarrow \infty$ . The behavior of current in the vicinity of this maximum at  $\alpha \gg 1$  is described by Eq. (46). It is also worth noticing that for  $\alpha \sim 1$ , the value given by Eq. (48) is close to the value of maxima at points  $\mathbf{r}_{00}^{\text{II}}$ ,  $\mathbf{r}_{00}^{\text{I}}$ . Therefore, the vector density plot shows a red circular band [see Fig. 6(b)].

Analogously, one can calculate the optically induced static potential:

$$\frac{e\phi_{\text{DC}}}{m} = \frac{2\pi^2 l^4 s^2}{d^4} \frac{e^{-2q_0 a}}{\Omega^2 + \Gamma^2/4} \{ \cos(2q_0 x) + \cos(2q_0 y) - 4\alpha [\cos(q_0 x) + \cos(q_0 y)] \}. \quad (49)$$

As one can see from this equation, the maximal optically induced voltage drop across different points of the unit cell of the periodic voltage structures is proportional to the amplitude of the circulating DC current  $e\delta\phi_{\text{DC}}^{\text{max}} \sim j_{\text{DC}S}/N_0$ .

### C. Optically induced magnetic field

The stationary radiation-induced magnetic field obeys

$$[\nabla \times \mathbf{H}] = \frac{4\pi e \mathbf{j}_{\text{DC}}(\mathbf{r})}{c} \delta(z). \quad (50)$$

Substituting  $\mathbf{H} = [\nabla \times \mathbf{A}]$  ( $\text{div} \mathbf{A} = 0$ ) and making Fourier transform over  $\mathbf{r}$ , we find

$$k^2 \mathbf{A}_{\mathbf{k}} - \frac{d^2 \mathbf{A}_{\mathbf{k}}}{dz^2} = \frac{4\pi e \mathbf{j}_{\text{DC}}^{\mathbf{k}}}{c} \delta(z). \quad (51)$$

Finite at  $|z| \rightarrow \infty$  solution of this equation reads  $\mathbf{A}_{\mathbf{k}}(z) = (2\pi e/c k) \mathbf{j}_{\text{DC}}^{\mathbf{k}} \exp(-k|z|)$ . Hence, the Fourier transform of the vector potential (and, consequently, of the magnetic field) is proportional to the Fourier transform of the DC current. In the vicinity of plasmonic peaks, only several  $\mathbf{k}$  satisfying resonant conditions contribute to the current and magnetic field, so spatial dependence of the field is found by the summation over these discrete set of  $\mathbf{k}$ .

Let us, for example, calculate the perpendicular component of the field,  $H_z$ , in the fundamental mode within the resonance approximation. In this case,  $\mathbf{k}$  runs over  $(\pm q_0, \pm q_0)$  for the plasmonic contribution and over  $(\pm q_0, 0)$  and  $(0, \pm q_0)$  for the mixed contribution [see Eqs. (40) and (41)]. Instead of summation over these  $\mathbf{k}$ , one can take into account that all terms in  $\pi(\mathbf{r})$  and  $\mu(\mathbf{r})$  are eigenfunctions of the Laplace operator,  $\Delta$ , and present the field in the operator form as

$$H_z(\mathbf{r}, z) = \frac{e^{-\sqrt{-\Delta}|z|}}{\sqrt{-\Delta}} \frac{2\pi e \mathbf{e}_z [\nabla \times \mathbf{j}_{\text{DC}}(\mathbf{r})]}{c}. \quad (52)$$

From this equation and Eq. (43), we find

$$H_z(\mathbf{r}, z) = -\frac{4\pi e}{c} \frac{1}{\Omega^2 + \Gamma^2/4} \times \left\{ \pi_0 \cos(q_0 x) \cos(q_0 y) \frac{e^{-\sqrt{2}q_0|z|}}{\sqrt{2}} + \mu_0 \Omega [\cos(q_0 x) + \cos(q_0 y)] e^{-\sqrt{q_0}|z|} \right\}. \quad (53)$$

Figure 7 shows the density plot of the magnetic field in the 2DEL plane:

$$H_z(\mathbf{r}, 0) = -\frac{\sqrt{32}\pi e j_0}{c} \frac{e^{-2q_0 a}}{\Omega^2 + \Gamma^2/4} \left\{ \cos(q_0 x) \cos(q_0 y) + \frac{\alpha}{\sqrt{2}} [\cos(q_0 x) + \cos(q_0 y)] \right\}. \quad (54)$$

For  $\alpha \ll 1$ , the field has maxima (within the area  $0 < x < d$ ,  $0 < y < d$ ) at the points  $(0, 0)$ ,  $(d, 0)$ ,  $(0, d)$ ,  $(d/2, d/2)$ ,  $(d, d)$  where  $\cos(q_0 x) \cos(q_0 y)$  is maximal [these maxima have equal heights and correspond to centers of red circles in Fig. 7(a)]. With increasing  $\alpha$ , the amplitude of the central maximum at  $(d/2, d/2)$  decreases by the factor  $1 - 2\alpha$  (for  $\alpha > 1$  this maximum transforms into minimum), while the amplitude of the other four maxima is increased by the factor  $1 + 2\alpha$ . Hence, for  $\alpha \gg 1$ , the field has four equivalent maxima at the points  $(0, 0)$ ,  $(d, 0)$ ,  $(0, d)$ ,  $(d, d)$  corresponding to the maxima of both  $\cos(q_0 x) + \cos(q_0 y)$  and  $\cos(q_0 x) \cos(q_0 y)$  [the maxima correspond to centers of red circles in Fig. 7(c)].

## V. DISCUSSION

### A. Finite viscosity, external magnetic field, and finite size effects

Above, we presented calculations for zero external magnetic field for an ideal infinite 2DEL with zero viscosity. The detailed analysis of different magnetoresponse regimes of the viscous electron liquid in the system under discussion is out of the scope of this paper and will be presented elsewhere. Here, we limit ourselves to the simplest but at the same time the most interesting case of the resonant excitation, when some of the plasmonic modes with wave vectors given by Eq. (17) satisfy the resonance condition:  $\omega \approx \omega_{nm}$ , where  $\omega_{nm}$  is given by Eq. (19). In this case, within the resonant approximation, the effect of a weak magnetic field,  $B$ , with  $\omega_c \ll \omega$  ( $\omega_c = eB/mc$  is the cyclotron frequency) can be accounted for by replacing  $\omega_{nm}^2$  with

$$\omega_{nm}^2(B) = \omega_{nm}^2 + \omega_c^2. \quad (55)$$

Hence, a weak magnetic field shifts the positions of the resonances shown in Fig. 4, thus giving an additional way to control the DC current and magnetization.

Within the same resonance approximation, the effect of a weak viscosity, satisfying the inequality  $\nu q_{nm}^2 \ll \omega$ , is accounted by replacing elastic damping  $\gamma$  with

$$\gamma_{nm} = \gamma + \nu q_{nm}^2. \quad (56)$$

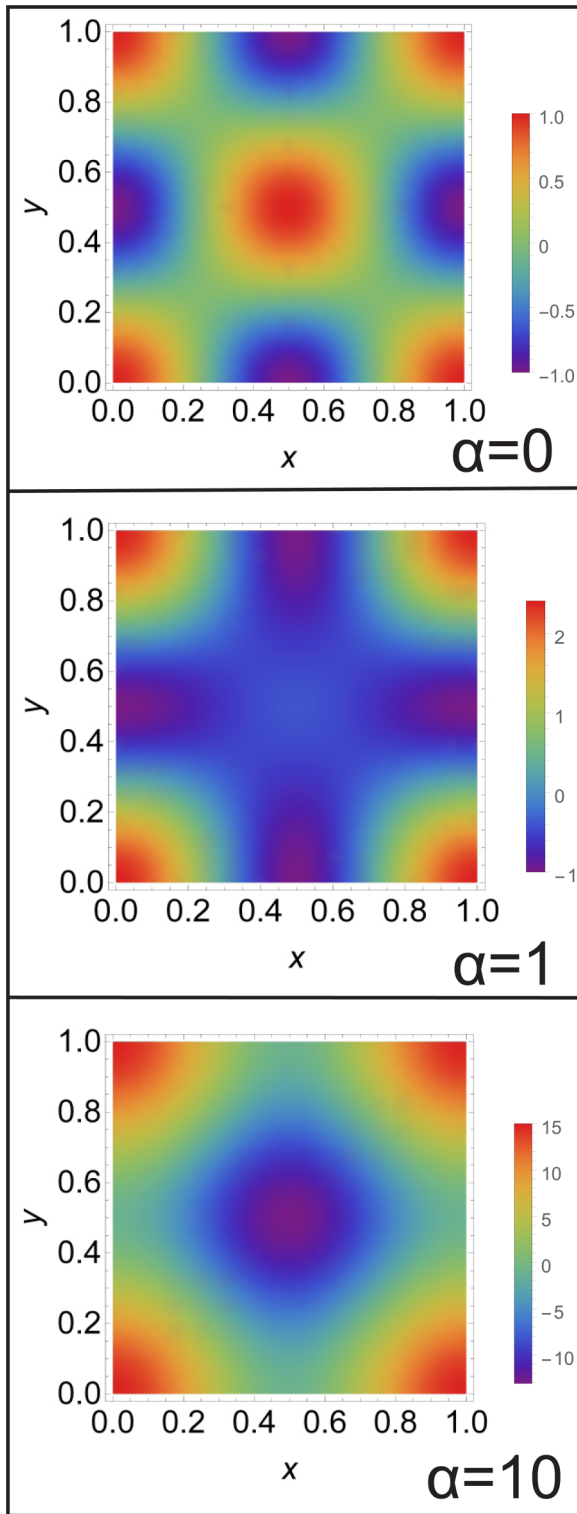


FIG. 7. Density plot of  $H_z(\mathbf{r}, 0)$  for different values of parameter  $\alpha = 2\Omega\mu_0/\pi_0$  (here,  $x$  and  $y$  are measured in units of  $d$ ).

The resonance is described by Eq. (22) with

$$\Omega \approx \frac{\omega - \omega_{nm}(B)}{\omega_{nm}(B)}, \quad \Gamma \approx \frac{\gamma_{nm}}{\omega_{nm}}. \quad (57)$$

As seen from Eq. (56), the measurement of widths of two plasmonic resonances with different resonance frequencies

( $\omega_{n_1 m_1} \neq \omega_{n_2 m_2}$ ) allows one to extract the value of  $\nu$ :

$$\nu = \frac{(\gamma_{n_1 m_1} - \gamma_{n_2 m_2})d^2}{(2\pi)^2(n_1^2 + m_1^2 - n_2^2 - m_2^2)}. \quad (58)$$

Evidently, one can also extract the momentum relaxation time by measuring  $\gamma_{n_1 m_1}$  and  $\gamma_{n_2 m_2}$ . It is worth noting that Eq. (58) does not include any characteristic of the material and depends on a single geometrical factor—the distance between nanospheres, which can be well controlled in experiment. Hence, the HIFE gives a direct way to extract the electron viscosity.

In this paper, we considered an infinite 2D system. An interesting question is related to finite-size effects, i.e., to the behavior of the current and magnetic field at the boundary of the system. A detailed discussion of this issue is beyond the scope of this paper and will be studied elsewhere. Here we restrict ourselves to a few comments. One can consider the situation when a diffraction square lattice having a finite size  $L = Nd$ , (here  $N \gg 1$  is an integer number) is located over an infinite 2D plane. Then, when calculating the function  $Z(\mathbf{r})$  in integrals over  $dq_i$  ( $i = x, y$ ), the factors  $\sin(q_i L/2)/\sin(q_i d/2)$  appear, which describe the smearing of  $\mathbf{q}$  around the quantized vectors of inverse lattice of  $\mathbf{q}_{nm}$  [see Eq. (17)] by values of the order of  $\delta q_i \sim 1/L$ . Considering the fundamental mode and calculating the corresponding integrals, one can show that outside of the region covered by diffraction lattice, the plasmonic and mixed contributions exponentially decay with different exponents,

$$\pi(\mathbf{r}) \propto \exp(-\delta r/L_\pi), \quad \mu(\mathbf{r}) \propto \exp(-\delta r/L_\mu),$$

where  $\delta r$  is distance from the edge of the diffraction region,  $L_\pi = 1/\sqrt{k_0 Q} = s/\sqrt{\omega_0 \gamma}$ , and  $L_\mu = 1/Q = s/\gamma$ . It is worth noting that for a small damping rate, both  $L_\pi$  and  $L_\mu$  might become on the order or even larger than  $L$ , which means that for sufficiently clean 2DEL the circular current and magnetic field can appear well beyond the region covered by diffraction lattice.

### B. Estimates of relevant parameters for various structures

In this section, we present some estimates of the relevant physical parameters for various materials and briefly discuss applicability of our approximations for realistic structures. We use the following geometrical parameters:  $d = 250$  nm,  $a = 50$  nm,  $R = 25$  nm. The plasma wave velocity is estimated by using a standard equation [16] and assuming that there is the back gate in the system. The barrier (spacer) width given in Table I corresponds to the typical values for each material system. The electric field of the incoming radiation is taken as  $E_0 = 10^5$  V/cm. We estimate both current  $j_0$ , which characterizes the current flow for the nonresonant case when the quality factor is on the order of unity, and also the current

$$j_{\text{DC}}^m = \frac{8j_0}{\Gamma^2} \exp^{-4\pi a/d}, \quad (59)$$

which is much larger than  $j_0$  for sharp resonances, when  $\Gamma \ll 1$  [see Eq. (45)]. For estimates of plasmonic-enhanced

TABLE I. The estimated parameters for different structures.

	Barrier thickness (nm)	$T$ (k)	2D carrier density ( $1/\text{cm}^2$ )	$f = \omega_0/2\pi$ (THz)	$\gamma/\omega_0$	$e j_0$ (A/m)	$j_{\text{DC}}^m/j_0$	$e j_{\text{DC}}^m$ (A/m)	$H^m$ (Gs)
GaN	20	300	$10^{13}$	7	0.087	0.1	87	9	0.086
GaN	20	77	$10^{13}$	7	0.005	0.1	21897	2299	20.4
Si	4	300	$2 \times 10^{12}$	2.3	0.4	0.84	3.5	3	0.025
Si	4	77	$2 \times 10^{12}$	2.3	0.03	0.84	657	550	4.9
InGaAs	20	300	$2 \times 10^{12}$	6.4	0.089	0.89	84	74	0.64
InGaAs	20	77	$2 \times 10^{12}$	6.4	0.03	0.88	701	618	5.5
p diamond	4	300	$2 \times 10^{12}$	1	0.08	0.8	112	89	0.78
p-diamond	4	77	$2 \times 10^{12}$	1	0.01	0.8	4815	3814	34

magnetic field, we use

$$H^m = \frac{16\sqrt{2}\pi e j_0}{c\Gamma^2} \exp^{-4\pi a/d} \quad (60)$$

[see Eq. (54)].

Table I lists the calculated values of the most important parameters, i.e., fundamental frequency, quality factor, characteristic value of the DC current, and maximal magnetic field. For all the materials listed in this table, the frequency of the fundamental plasmonic mode is in the THz range. The value of the optically induced magnetic field can be sufficiently large at not-too-low temperatures, 77 K, especially in the GaN and p-diamond-based structures. For these estimates, we used material parameters listed in Table II with references to corresponding experiments and/or numerical simulations. Using the numbers, presented in the tables, we can discuss validity of approximations used in our calculations.

In our model, we assumed that the spheres comprising the plasmonic coupler are fully polarized. This implies that internal plasmonic frequency of the nanospheres is very large compared to characteristic frequencies of the problem. The condition is well satisfied, provided that frequency of three-dimensional plasma oscillations in the metal, which the spheres are made from,  $\omega_{3D}$ , is large as compared to typical plasmonic frequency in our problem, which is the fundamental frequency  $\omega_0$  [see Eq. (20)]. For typical values of plasma wave velocity in 2D gated InGaAs-based structure, [16], and  $d = 250$  nm, we get  $f_0 = \omega_0/2\pi = 6.4$  THz (see Table I and Fig. 8). At the same time, the 3D plasmonic frequencies in metal are at least two orders of magnitude higher due to very high electron concentration. For example, a simple estimate for silver, with 3D concentration  $6 \times 10^{22} \text{ cm}^{-3}$ , yields for  $\omega_{3D}$  value about  $10^{16} \text{ s}^{-1}$ .

Let us now estimate spatial scales shown in Fig. 2. Assuming the frequency of the radiation to be  $\omega = 3 \times 10^{13} \text{ s}^{-1}$  (which corresponds to  $f = \omega/2\pi = 5$  THz), and using the

estimate for typical plasma wave velocity  $1.6 \times 10^8 \text{ cm/s}$ , we find  $\lambda_0 = 250$  nm. Rewriting damping length as  $Q^{-1} = \lambda_0(\omega_0/\gamma\pi)$  and using data of Table I for InGaAs at  $T = 77$  K, we estimate  $Q^{-1} \approx 3500$  nm. This justifies ordering of the spatial scales in Fig. 2. As seen from Table I, for other materials we also have  $Q^{-1} \gg \lambda_0$ .

Finally, we present a picture of the current for parameters of an InGaAs-based structure with  $d = 5a = 10R = 250$  nm, for two temperatures, 300 and 77 K (see Fig. 8). We see resonance at the fundamental frequency  $f = f_0 = \omega_0/2\pi$  and the next one at the frequency  $\sqrt{2}f_0$ . As expected, the quality factor of plasmonic resonances increases with decreasing temperature.

## VI. CONCLUSION

To conclude, we predicted excitation of circular plasmonic modes (twisted plasmons) in 2DEL by circularly polarized electromagnetic wave via a plasmonic coupler made of periodically placed nanospheres. We demonstrated that rectification of the plasmons leads to a helicity-sensitive circular DC current, and consequently, to a magnetic moment, thus demonstrating the HIFE. This effect is dramatically increased in the vicinity of plasmonic resonances, so the DC current shows sharp plasmonic peaks. There are two interfering contributions to the peaks, the plasmonic contribution and the contribution involving both the plasmonic and the Drude excitations. As a result, plasmonic resonances have an asymmetric Fano-like shape. The suggested system can be used for optical tunable magnetization of 2D systems for many optoelectronic devices operating in the THz range of frequencies and for the characterization and parameter extraction of 2D electron liquids. In particular, measuring the widths of different plasmonic resonances allows one to extract the electron viscosity.

TABLE II. Material parameters used in the calculations.

	Effective mass	Mobility $\text{cm}^2/\text{Vs}$ (77k)	Mobility $\text{cm}^2/\text{Vs}$ (300k)	Dielectric constant of material	Dielectric constant of barrier
Silicon	0.19 [62]	20000 [60]	1450 [59]	11.9 [62]	3.9
GaN	0.23 [64]	31700 [55]	2000 [56]	8.9 [62]	8.9
InGaAs	0.041 [63]	35000 [61]	12000 [61]	13.9 [62]	12.1
p diamond	0.663 [58]	35000 [57]	5300 [57]	5.7 [62]	5.7

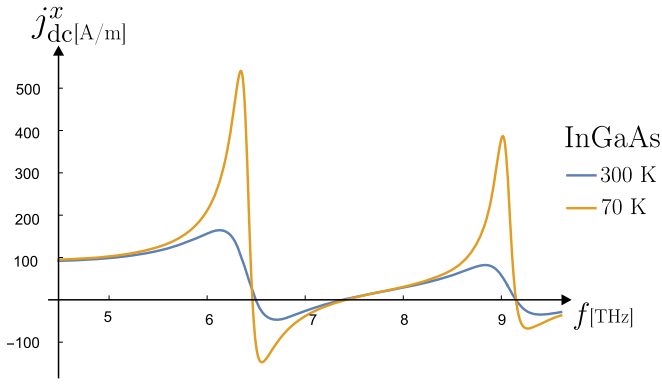


FIG. 8. Current-frequency dependence for parameters of InGaAs-based structure with  $d = 5a = 10R = 250$  nm at  $x = y = d/8$ , for two temperatures, 300 and 77 K.

### ACKNOWLEDGMENTS

The work of V.Yu.K. was supported by RFBR (Grant No. 20-02-00490), by Foundation for the Advancement of Theoretical Physics and Mathematics BASIS, and by the Foundation for Polish Science through Grant No. MAB/2018/9 for CENTERA. The work at RPI was supported by the U.S. Army Research Laboratory Cooperative Research Agreement (project monitor Dr. Meredith Reed) and by the US ONR (project monitor Dr. Paul Maki).

### APPENDIX A: LINEAR RESPONSE (TECHNICAL DETAILS)

Linearizing Eqs. (2) and (3) and making a Fourier transform, we get

$$-i\omega\delta n_{\omega\mathbf{q}} + i\mathbf{q}\delta\mathbf{v}_{\omega\mathbf{q}} = 0, \quad (\text{A1})$$

$$i\mathbf{q}s^2\delta n_{\omega\mathbf{q}} + (\gamma - i\omega)\delta\mathbf{v}_{\omega\mathbf{q}} = \frac{e(\mathbf{E}_0 + \mathbf{E}_1)_{\omega\mathbf{q}}}{m}, \quad (\text{A2})$$

where

$$\left(\frac{e\mathbf{E}_0}{m}\right)_{\omega\mathbf{q}} = \frac{eE_0}{2m}(\mathbf{e}_x - i\mathbf{e}_y)(2\pi)^2\delta(\mathbf{q}), \quad (\text{A3})$$

$$\left(\frac{e\mathbf{E}_1}{m}\right)_{\omega\mathbf{q}} = -\frac{\pi\mathbf{q}e^2p}{m}e^{-i\varphi_{\mathbf{q}}}e^{-qa}, \quad (\text{A4})$$

and  $e^{-i\varphi_{\mathbf{q}}} = (q_x - iq_y)/q$

The solution of Eqs. (A1) and (A2) reads

$$\delta n_{\omega\mathbf{q}} = 2\pi il^2 \frac{q^2}{q^2 - k^2} e^{-i\varphi_{\mathbf{q}}} e^{-qa}, \quad (\text{A5})$$

$$\begin{aligned} \delta\mathbf{v}_{\omega\mathbf{q}} &= 2\pi il^2 \frac{\omega\mathbf{q}}{q^2 - k^2} e^{-i\varphi_{\mathbf{q}}} e^{-qa} \\ &+ \frac{eE_0(\mathbf{e}_x - i\mathbf{e}_y)}{2m(\gamma - i\omega)} (2\pi)^2\delta(\mathbf{q}), \end{aligned} \quad (\text{A6})$$

where  $l$  and  $k$  are given by Eqs. (14) and (15) of the main text. Next, we find the Fourier transform of the velocity and concentration:

$$\delta n_{\omega}(\mathbf{r}) = \Delta Z(\mathbf{r}), \quad (\text{A7})$$

$$\delta\mathbf{v}_{\omega}(\mathbf{r}) = i\omega\nabla Z(\mathbf{r}) + \frac{eE_0(\mathbf{e}_x - i\mathbf{e}_y)}{2m(\gamma - i\omega)}, \quad (\text{A8})$$

where

$$\begin{aligned} Z(\mathbf{r}) &= -i2\pi l^2 \int \frac{d^2q}{(2\pi)^2} \frac{e^{i\mathbf{q}\mathbf{r}} e^{-i\varphi_{\mathbf{q}}} e^{-qa}}{q^2 - k^2} \\ &= l^2(x - iy)f(r). \end{aligned} \quad (\text{A9})$$

Function  $f(r)$  is given by

$$\begin{aligned} f(r) &= \int_0^\infty \frac{dq q J_1(qr) e^{-qa}}{r(q^2 - k^2)} \\ &\approx \frac{\pi}{2r} [\mathbb{H}_{-1}(kr) + iJ_1(kr)] - \frac{1}{r} \left(1 - \frac{r}{a + \sqrt{a^2 + r^2}}\right), \end{aligned} \quad (\text{A10})$$

where  $\mathbb{H}_{-1}$  and  $J_1$  are the Struve and Bessel functions. Here we assumed  $Q \ll k_0 \ll 1/a$  [54].

The asymptotes of the function  $f$  are given by

$$f \approx \begin{cases} \sqrt{\frac{\pi}{2kr^3}} e^{i(kr - \pi/4)} \left(1 + \frac{3i}{8kr}\right) - \frac{1}{k^2 r^3}, & r \gg 1/k_0 \\ \frac{1}{a + \sqrt{a^2 + r^2}} + \frac{i\pi k}{4}, & r \ll 1/k_0. \end{cases} \quad (\text{A11})$$

From Eqs. (24), (A7), and (A8), we get

$$\delta n_{\omega}^{\text{P}}(\mathbf{r}) = l^2(x - iy) \left[ f'' + \frac{3f'}{r} \right], \quad (\text{A12})$$

$$\delta\mathbf{v}_{\omega}^{\text{P}}(\mathbf{r}) = \omega l^2(x - iy) \left[ i \frac{(rf)'}{r} \mathbf{e}_r + \frac{f}{r} \mathbf{e}_\varphi \right], \quad (\text{A13})$$

$$\delta\mathbf{v}_{\omega}^{\text{D}}(\mathbf{r}) = \frac{eE_0(\mathbf{e}_x - i\mathbf{e}_y)}{2m(\gamma - i\omega)}. \quad (\text{A14})$$

As seen, the velocity oscillations can be presented as a sum of the  $f$ -dependent inhomogeneous contribution and the homogeneous Drude contribution, given, respectively, by Eqs. (A13) and (A14).

### APPENDIX B: EXPRESSIONS FOR $R_1^{\text{P}}$ AND $\Phi_2^{\text{P}}$ FOR A SINGLE NANOSPHERE

Using Eqs. (A10)–(A14) and (18), we find

$$R_1^{\text{P}} = -i\omega l^4 (rf'' + 3f')(rf^*) + \text{c.c.} \approx \pi\omega l^4 \begin{cases} \frac{k_0}{r} e^{-Qr}, & r > 1/k_0 \\ \frac{kor}{2(r^2 + a^2)^{3/2}}, & r < 1/k_0, \end{cases} \quad (\text{B1})$$

$$\Phi_1^{\text{P}} = \omega l^4 (rf'' + 3f')f^* + \text{c.c.} \approx \pi\omega l^4 \begin{cases} -\frac{k_0}{r^2} e^{-Qr}, & r > 1/k_0 \\ -\frac{2}{\pi} \frac{r}{(r^2 + a^2)^{3/2} (a + \sqrt{r^2 + a^2})}, & r < 1/k_0, \end{cases} \quad (\text{B2})$$

$$R_2^P = -\frac{\omega^2 l^4}{\gamma} [(rf^*)'(rf)'' + f^* f'] + \text{c.c.}$$

$$\approx \frac{\pi \omega^2 l^4}{\gamma} \begin{cases} \frac{k_0}{2r^2} (1 + Qr) e^{-Qr}, & r > 1/k_0 \\ \frac{2}{\pi} \frac{r}{(a + \sqrt{r^2 + a^2})^3} \left[ \frac{a^3}{(a^2 + r^2)^2} + \frac{r^2 + 3a^2}{(a^2 + r^2)^{3/2}} \right], & r < 1/k_0, \end{cases} \quad (\text{B3})$$

$$\Phi_2^P = 0. \quad (\text{B4})$$

### APPENDIX C: EXPRESSIONS FOR $R_i^M$ AND $\Phi_i^M$ FOR A SINGLE NANOSPHERE

By direct averaging of  $\delta n^P \delta \mathbf{v}^D$  over time, we get

$$R_1^M - i\Phi_1^M = \frac{2l^4 s^2}{R^3} \frac{rf'' + 3f'}{\gamma + i\omega}. \quad (\text{C1})$$

In the limiting cases, assuming  $\omega \gg \gamma$  and taking in all terms in lowest nonzero order with respect to  $\gamma/\omega$ , we get

$$R_1^M = \frac{2l^4 s^2}{R^3} \begin{cases} \frac{\sqrt{\pi} k_0^{3/2} e^{-Qr/2} \cos(k_0 r + \frac{\pi}{4})}{\omega \sqrt{2r}}, & r > 1/k_0 \\ -\frac{\gamma}{\omega^2} \frac{r}{(r^2 + a^2)^{3/2}}, & r < 1/k_0 \end{cases} \quad (\text{C2})$$

and

$$\Phi_1^M = -\frac{2l^4 s^2}{\omega R^3} \begin{cases} \frac{\sqrt{\pi} k_0^{3/2} e^{-Qr/2} \sin(k_0 r + \frac{\pi}{4})}{\sqrt{2r}}, & r > 1/k_0 \\ \frac{r}{(r^2 + a^2)^{3/2}}, & r < 1/k_0. \end{cases} \quad (\text{C3})$$

Finally, from Eqs. (18), (A13), and (A14), we find (in lowest order with respect to  $\gamma/\omega$ )

$$R_2^M = -\frac{l^4 s^2}{\gamma R^3} (rf'' + 3f') + \text{c.c.}$$

$$= \frac{2l^4 s^2}{\gamma R^3} \begin{cases} \frac{\sqrt{\pi} k_0^{3/2} e^{-Qr/2} \sin(k_0 r + \frac{\pi}{4})}{\sqrt{2r}}, & r > 1/k_0 \\ \frac{r}{(a^2 + r^2)^{3/2}}, & r < 1/k_0, \end{cases} \quad (\text{C4})$$

$$\Phi_2^M = 0. \quad (\text{C5})$$

### APPENDIX D: ASYMPTOTICAL VALUES OF $j_{\text{DC}}$ AND $E_{\text{DC}}$ FOR A SINGLE NANOSPHERE

Using Eqs. (B1)–(B4) and (C2)–(C5), we find asymptotical behavior of  $j_{\text{DC}}$  and  $E_{\text{DC}}$ , accounting both plasmonic and mixed contributions,

$$j^{\text{DC}} = -\frac{\omega l^4 N_0}{a^3} \begin{cases} A\left(\frac{r}{a}\right) + \frac{a}{R^3 k_0^2} C\left(\frac{r}{a}\right), & r \ll 1/k_0 \\ \frac{\pi a^3}{r^3} \left[ k_0 r e^{-Qr} + \sqrt{\frac{2}{\pi k_0 r}} \left(\frac{r}{R}\right)^3 e^{-Qr/2} \sin(k_0 r + \frac{\pi}{4}) \right], & 1/k_0 \ll r \ll \frac{\ln[k_0/Q]}{Q} \\ 6a^3 \left( -\frac{1}{k_0^2 r^7} + \frac{1}{R^3 k_0^4 r^4} \right), & \frac{\ln[k_0/Q]}{Q} \ll r, \end{cases} \quad (\text{D1})$$

$$\frac{eE^{\text{DC}}}{m} = -\frac{\omega^2 l^4}{a^3} \begin{cases} \pi B\left(\frac{r}{a}\right) + \frac{a}{R^3 k_0^2} C\left(\frac{r}{a}\right), & r \ll 1/k_0 \\ \frac{\pi a^3}{r^3} \left[ \frac{k_0 r}{2} e^{-Qr} + \sqrt{\frac{2}{\pi k_0 r}} \left(\frac{r}{R}\right)^3 e^{-Qr/2} \sin(k_0 r + \frac{\pi}{4}) \right], & 1/k_0 \ll r \ll \frac{\ln[k_0/Q]}{Q} \\ 6a^3 \left( \frac{5}{k_0^2 r^7} + \frac{1}{R^3 k_0^4 r^4} \right), & \frac{\ln[k_0/Q]}{Q} \ll r, \end{cases} \quad (\text{D2})$$

where

$$A(x) = \frac{2x}{(1+x^2)^{3/2} (1+\sqrt{1+x^2})}, \quad (\text{D3})$$

$$B(x) = \frac{2x}{(1+\sqrt{1+x^2})^3} \frac{1+(3+x^2)\sqrt{1+x^2}}{(1+x^2)^2},$$

$$C(x) = \frac{2x}{(1+x^2)^{3/2}}. \quad (\text{D4})$$

### APPENDIX E: EXPRESSIONS FOR $\mathbf{J}_i^P$ , $\mathbf{J}_i^M$ FOR PERIODIC ARRAY OF NANOSPHERES

For a periodic array of nanospheres, one should replace  $Z(\mathbf{r})$  with the following sum:

$$\sum_{n,m} Z(\mathbf{r} - \mathbf{r}_{nm}) = \sum_{n,m} \int \frac{d^2\mathbf{q}}{(2\pi)^2} Z_{\mathbf{q}} e^{-i\mathbf{q}\mathbf{r}_{nm}} e^{i\mathbf{q}\mathbf{r}}, \quad (\text{E1})$$

where  $Z(\mathbf{r})$  is given by Eq. (13) and

$$\mathbf{r}_{nm} = d(n\mathbf{e}_x + m\mathbf{e}_y) \quad (\text{E2})$$

are lattice vectors of the squared array. Next, we use the Poisson summation formula:

$$\begin{aligned} \sum_{n,m} e^{-i\mathbf{q}\mathbf{r}_{nm}} &= \sum_n e^{-idq_x n} \sum_m e^{-idq_y m} \\ &= \left(\frac{2\pi}{d}\right)^2 \sum_m \delta\left(q_x - \frac{2\pi m}{d}\right) \sum_n \delta\left(q_y - \frac{2\pi n}{d}\right). \end{aligned} \quad (\text{E3})$$

Substituting Eq. (E3) into Eq. (E1) and integrating over  $d^2\mathbf{q}$ , we get

$$\sum_{n,m} Z(\mathbf{r} - \mathbf{r}_{nm}) = \frac{1}{d^2} \sum_{\mathbf{q}=\mathbf{q}_{nm}} Z_{\mathbf{q}} e^{i\mathbf{q}\mathbf{r}}, \quad (\text{E4})$$

where inverse lattice vectors  $\mathbf{q}_{nm}$  are given by Eq. (17).

The rectified currents  $\mathbf{J}_i^P$  are given by double sums over  $\mathbf{q}$ ,  $\mathbf{q}'$  (both  $\mathbf{q}$  and  $\mathbf{q}'$  run over values  $\mathbf{q}_{nm}$ ), while  $\mathbf{J}_i^M$  by ordinary ones. For convenience of further calculations, in plasmonic contribution we introduce Kronecker symbol  $\delta_{\mathbf{Q},\mathbf{q}-\mathbf{q}'}$  and sum over  $\mathbf{Q}$ :

$$\mathbf{J}_1^P(\mathbf{r}) = \sum_{\mathbf{Q}} e^{i\mathbf{Q}\mathbf{r}} \mathbf{J}_{1\mathbf{Q}}^P + \text{c.c.} = \frac{4\pi^2 l^4}{d^4} \sum_{\mathbf{Q}} e^{i\mathbf{Q}\mathbf{r}} \sum_{\mathbf{q},\mathbf{q}'} \delta_{\mathbf{Q},\mathbf{q}-\mathbf{q}'} \frac{e^{-i(\varphi_{\mathbf{q}} - \varphi_{\mathbf{q}'}) - a(q+q')}}{(q^2 - k^2)(q'^2 - k'^2)} \omega \mathbf{q} \mathbf{q}'^2 + \text{c.c.}, \quad (\text{E5})$$

$$\mathbf{J}_2^P(\mathbf{r}) = \sum_{\mathbf{Q}} e^{i\mathbf{Q}\mathbf{r}} \mathbf{J}_{2\mathbf{Q}}^P + \text{c.c.} = \frac{4i\pi^2 l^4}{d^4 \gamma} \sum_{\mathbf{Q}} e^{i\mathbf{Q}\mathbf{r}} \sum_{\mathbf{q},\mathbf{q}'} \delta_{\mathbf{Q},\mathbf{q}-\mathbf{q}'} \frac{e^{-i(\varphi_{\mathbf{q}} - \varphi_{\mathbf{q}'}) - a(q+q')}}{(q^2 - k^2)(q'^2 - k'^2)} \omega^2 (\mathbf{q}\mathbf{q}')^{\mathbf{q}'} + \text{c.c.}, \quad (\text{E6})$$

$$\mathbf{J}_1^M(\mathbf{r}) = \sum_{\mathbf{Q}} e^{i\mathbf{Q}\mathbf{r}} \mathbf{J}_{1\mathbf{Q}}^M + \text{c.c.} = \frac{2i\pi l^4 s^2}{d^2 R^3} \frac{1}{\gamma + i\omega} \sum_{\mathbf{Q}} \frac{e^{i\mathbf{Q}\mathbf{r} - i\varphi_{\mathbf{Q}} - aQ}}{(Q^2 - k^2)} (\mathbf{e}_x + i\mathbf{e}_y) + \text{c.c.}, \quad (\text{E7})$$

$$\mathbf{J}_2^M(\mathbf{r}) = \sum_{\mathbf{Q}} e^{i\mathbf{Q}\mathbf{r}} \mathbf{J}_{2\mathbf{Q}}^M + \text{c.c.} = \frac{2\pi l^4 s^2}{d^2 R^3 \gamma} \frac{1}{\gamma + i\omega} \sum_{\mathbf{Q}} \frac{e^{i\mathbf{Q}\mathbf{r}} e^{-aQ} \omega \mathbf{Q} \mathbf{Q}}{Q^2 - k^2} + \text{H.c.} \quad (\text{E8})$$

Using Eqs. (31) and (32), we find expressions for the optically induced DC current, which includes both plasmonic and mixed contributions:

$$\begin{aligned} \mathbf{j}^{\text{DC}} &= N_0 \frac{4\pi^2 l^4}{d^4} \left\{ \omega \sum_{\mathbf{q},\mathbf{q}'} \frac{[\mathbf{e}_z \times (\mathbf{q} - \mathbf{q}')] \cdot (\mathbf{e}_z \times (\mathbf{q} - \mathbf{q}'))}{|\mathbf{q} - \mathbf{q}'|} \left( \frac{[\mathbf{e}_z \times (\mathbf{q} - \mathbf{q}')] \cdot \mathbf{q}}{|\mathbf{q} - \mathbf{q}'|} \right) \frac{q'^2 e^{i(\mathbf{q}-\mathbf{q}')\mathbf{r}} e^{-i(\varphi_{\mathbf{q}} - \varphi_{\mathbf{q}'}) - a(q+q')}}{(q^2 - k^2)(q'^2 - k'^2)} \right. \\ &\quad \left. + \frac{i s^2 d^2}{2\pi R^3} \frac{1}{\gamma + i\omega} \sum_{\mathbf{Q}} \frac{[\mathbf{e}_z \times \mathbf{Q}] \cdot (\mathbf{e}_z \times \mathbf{Q}) (\mathbf{e}_x + i\mathbf{e}_y)}{Q} \left( \frac{[\mathbf{e}_z \times \mathbf{Q}] \cdot \mathbf{Q}}{Q} \right) \frac{Q^2 e^{i\mathbf{Q}\mathbf{r} - i\varphi_{\mathbf{Q}} - aQ}}{Q^2 - k^2} \right\} + \text{c.c.}, \end{aligned} \quad (\text{E9})$$

$$\frac{e\mathbf{E}_{\text{DC}}}{m} = \gamma \sum_{\mathbf{Q}} \frac{\mathbf{Q}}{Q} \left\{ \frac{\mathbf{Q}}{Q} [\mathbf{J}_{1\mathbf{Q}}^P + \mathbf{J}_{2\mathbf{Q}}^P + \mathbf{J}_{1\mathbf{Q}}^M + \mathbf{J}_{2\mathbf{Q}}^M] \right\} e^{i\mathbf{Q}\mathbf{r}} + \text{c.c.}, \quad (\text{E10})$$

$$\approx (\text{for } \gamma \ll \omega) \approx \gamma \sum_{\mathbf{Q}} \frac{\mathbf{Q}}{Q} \left\{ \frac{\mathbf{Q}}{Q} [\mathbf{J}_{2\mathbf{Q}}^P + \mathbf{J}_{2\mathbf{Q}}^M] \right\} e^{i\mathbf{Q}\mathbf{r}} + \text{c.c.}, \quad (\text{E11})$$

$$= \frac{4\pi^2 l^4}{d^4} \left\{ i\omega^2 \sum_{\mathbf{q},\mathbf{q}'} \frac{\mathbf{q} - \mathbf{q}'}{|\mathbf{q} - \mathbf{q}'|} \left[ \frac{(\mathbf{q} - \mathbf{q}') \cdot \mathbf{q}'}{|\mathbf{q} - \mathbf{q}'|} \right] \frac{(\mathbf{q}\mathbf{q}') e^{i(\mathbf{q}-\mathbf{q}')\mathbf{r}} e^{-i(\varphi_{\mathbf{q}} - \varphi_{\mathbf{q}'}) - a(q+q')}}{(q^2 - k^2)(q'^2 - k'^2)} - i \frac{s^2 d^2}{2\pi R^3} \sum_{\mathbf{Q}} \frac{\mathbf{Q} \mathbf{Q} e^{i\mathbf{Q}\mathbf{r} - aQ}}{Q^2 - k^2} \right\} + \text{c.c.} \quad (\text{E12})$$

### APPENDIX F: EXPRESSIONS FOR RECTIFIED CURRENTS IN THE FUNDAMENTAL PLASMONIC MODE

For  $(n, m) = (1, 0), (0, 1), (-1, 0), (0, -1)$ , we have  $q = q_0 = 2\pi/d$ . Simple calculations yield

$$\mathbf{J}_1^P = \frac{32\pi^2 l^4}{d^4} \frac{\omega q_0^3 [\sin(q_0 y) \cos(q_0 x) \mathbf{e}_x - \sin(q_0 x) \cos(q_0 y) \mathbf{e}_y]}{|q_0^2 - k^2|^2} e^{-2q_0 a}, \quad (\text{F1})$$

$$\mathbf{J}_2^P = \frac{32\pi^2 l^4}{d^4} \frac{\omega^2 q_0^3 [\sin(q_0 x) \cos(q_0 x) \mathbf{e}_x + \sin(q_0 y) \cos(q_0 y) \mathbf{e}_y]}{\gamma |q_0^2 - k^2|^2} e^{-2q_0 a}, \quad (\text{F2})$$

$$\mathbf{J}_1^M = \frac{4\pi l^4}{d^2 R^3} \frac{q_0^2 \omega}{k_*^2 (q_0^2 - k^2)} [i \sin(q_0 x) + \sin(q_0 y)] (\mathbf{e}_x + i \mathbf{e}_y) e^{-q_0 a} + \text{c.c.}, \quad (\text{F3})$$

$$\mathbf{J}_2^M = \frac{4\pi l^4}{d^2 R^3} \frac{q_0^2 \omega^2}{\gamma k_*^2 (q_0^2 - k^2)} [\sin(q_0 x) \mathbf{e}_x + \sin(q_0 y) \mathbf{e}_y] e^{-q_0 a} + \text{c.c.} \quad (\text{F4})$$

Next, we substitute these equations into Eqs. (32) and (33). The latter can be written in the operator form

$$\mathbf{j}_{\text{DC}} = N_0 \frac{-\nabla \text{div} + \Delta}{\Delta} (\mathbf{J}_1^P + \mathbf{J}_1^M), \quad (\text{F5})$$

$$\frac{e \mathbf{E}_{\text{DC}}}{m} = \gamma \frac{\nabla}{\Delta} \text{div} (\mathbf{J}_1^P + \mathbf{J}_1^M + \mathbf{J}_2^P + \mathbf{J}_2^M), \quad (\text{F6})$$

$$\frac{e \phi_{\text{DC}}}{m} = \gamma \frac{1}{\Delta} \text{div} (\mathbf{J}_1^P + \mathbf{J}_1^M + \mathbf{J}_2^P + \mathbf{J}_2^M). \quad (\text{F7})$$

From Eqs. (F1)–(F7), we find

$$\mathbf{j}_{\text{DC}} = N_0 \left\{ \frac{16\pi^2 l^4}{d^4} \frac{\omega q_0^3 e^{-2q_0 a} [\sin(q_0 y) \cos(q_0 x) \mathbf{e}_x - \sin(q_0 x) \cos(q_0 y) \mathbf{e}_y]}{|q_0^2 - k^2|^2} + \frac{4\pi l^4}{d^2 R^3} \frac{\omega q_0^2 e^{-q_0 a} [\sin(q_0 y) \mathbf{e}_x - \sin(q_0 x) \mathbf{e}_y]}{k_*^2 (q_0^2 - k^2)} \right\} + \text{c.c.} \quad (\text{F8})$$

Close to resonance, this equation can be simplified and written in the form of Eq. (22) with  $\boldsymbol{\pi}$  and  $\boldsymbol{\mu}$  given by Eqs. (40) and (41), respectively. We also find (for  $\gamma \ll \omega$ )

$$\frac{e \mathbf{E}_{\text{DC}}}{m} = \left\{ \frac{16\pi^2 l^4}{d^4} \frac{\omega^2 q_0^3 e^{-2q_0 a} [\sin(q_0 x) \cos(q_0 x) \mathbf{e}_x + \sin(q_0 y) \cos(q_0 y) \mathbf{e}_y]}{|q_0^2 - k^2|^2} + \frac{4\pi l^4}{d^2 R^3} \frac{\omega^2 q_0^2 e^{-q_0 a} [\sin(q_0 x) \mathbf{e}_x + \sin(q_0 y) \mathbf{e}_y]}{k_*^2 (q_0^2 - k^2)} \right\} + \text{c.c.}, \quad (\text{F9})$$

$$\frac{e \phi_{\text{DC}}}{m} = \left\{ \frac{4\pi^2 l^4}{d^4} \frac{\omega^2 q_0^2 e^{-2q_0 a} [\cos(2q_0 x) + \cos(2q_0 y)]}{|q_0^2 - k^2|^2} + \frac{4\pi l^4}{d^2 R^3} \frac{\omega^2 q_0 e^{-q_0 a} [\cos(q_0 x) + \cos(q_0 y)]}{k_*^2 (q_0^2 - k^2)} \right\} + \text{c.c.} \quad (\text{F10})$$

- 
- [1] L. P. Pitaevskii, J. Exp. Theor. Phys. **39**, 1450 (1960) [Sov. Phys. JETP **12**, 1008 (1961)].
- [2] J. P. van der Ziel, P. S. Pershan, and L. D. Malmstrom, *Phys. Rev. Lett.* **15**, 190 (1965).
- [3] A. V. Kimel, A. Kirilyuk, P. A. Usachev, R. V. Pisarev, A. M. Balbashov, and Th. Rasing, *Nature* **435**, 655 (2005).
- [4] A. Kirilyuk, A. V. Kimel, and T. Rasing, *Rev. Mod. Phys.* **82**, 2731 (2010).
- [5] A. Kirilyuk, A. V. Kimel, and Th. Rasing, *Philos. Trans. R. Soc. A* **369**, 3631 (2011).
- [6] O. V. Kibis, *Phys. Rev. Lett.* **107**, 106802 (2011).
- [7] O. V. Kibis, O. Kyriienko, and I. A. Shelykh, *Phys. Rev. B* **87**, 245437 (2013).
- [8] A. M. Alexeev, I. A. Shelykh, and M. E. Portnoi, *Phys. Rev. B* **88**, 085429 (2013).
- [9] F. K. Joibari, Ya. M. Blanter, and G. E. W. Bauer, *Phys. Rev. B* **90**, 155301 (2014).
- [10] A. M. Alexeev and M. E. Portnoi, *Phys. Rev. B* **85**, 245419 (2012).
- [11] V. V. Kruglyak and M. E. Portnoi, *Pis'ma v Zh. Tekh. Fiziki* **31**, 20 (2005) [*Tech. Phys. Lett.* **31**, 1047 (2005)].
- [12] V. V. Kruglyak, M. E. Portnoi, and R. J. Hicken, *J. Nanophotonics* **1**, 013502 (2007).
- [13] M. L. Polianski, *Phys. Rev. B* **80**, 241301(R) (2009).
- [14] K. L. Koshelev, V. Yu. Kachorovskii, and M. Titov, *Phys. Rev. B* **92**, 235426 (2015).
- [15] K. L. Koshelev, V. Yu. Kachorovskii, M. Titov, and M. S. Shur, *Phys. Rev. B* **95**, 035418 (2017).
- [16] M. I. Dyakonov and M. S. Shur, *Phys. Rev. Lett.* **71**, 2465 (1993).
- [17] E. L. Ivchenko and S. D. Ganichev, *Pisma v ZheTF* **93**, 752 (2011) [*JETP Lett.* **93**, 673 (2011)].
- [18] J. B. Khurgin, *Nat. Nanotechnol.* **10**, 2 (2015).
- [19] P. Nordlander, *Nat. Nanotechnol.* **8**, 76 (2013).
- [20] J. Heber, *Nat. Mater.* **11**, 745 (2012).
- [21] A. N. Grigorenko, M. Polini, and K. S. Novoselov, *Nat. Photon.* **6**, 749 (2012).
- [22] F. H. L. Koppens, D. E. Chang, and F. J. Garcia de Abajo, *Nano Lett.* **11**, 3370 (2011).
- [23] D. K. Gramotnev and S. I. Bozhevolnyi, *Nature Photonics* **4**, 83 (2010).
- [24] S. A. Maier, *Plasmonics: Fundamentals and Applications* (Springer, NY, USA, 2007).
- [25] R. N. Gurzhi, *Usp. Fiz. Nauk* **94**, 689 (1968) [*Sov. Phys. Usp.* **11**, 255 (1968)].
- [26] M. J. M. de Jong and L. W. Molenkamp, *Phys. Rev. B* **51**, 13389 (1995).
- [27] M. I. Dyakonov and M. S. Shur, *Phys. Rev. B* **51**, 14341 (1995).

- [28] M. I. Dyakonov and M. S. Shur, *IEEE Trans. on Elec. Dev.* **43**, 380 (1996).
- [29] A. P. Dmitriev, A. S. Furman, and V. Yu. Kachorovskii, *Phys. Rev. B* **54**, 14020 (1996).
- [30] A. P. Dmitriev, A. S. Furman, V. Yu. Kachorovskii, G. G. Samsonidze, and Ge. G. Samsonidze, *Phys. Rev. B* **55**, 10319 (1997).
- [31] T. Otsuji and M. S. Shur, *IEEE Microwave Mag.* **15**, 43 (2014).
- [32] W. Knap, D. B. But, N. Dyakonova, D. Coquillat, A. Gutin, O. Klimenko, S. Blin, F. Teppe, M. S. Shur, T. Nagatsuma, S. D. Ganichev, and T. Otsuji, *Recent Results on Broadband Nanotransistor Based THz Detectors*, edited by C. Corsi, F. Sizov, NATO Science for Peace and Security Series B, Physics and Biophysics: THz and Security Applications (Springer, Dordrecht, Netherlands, 2014).
- [33] R. Jaggi, *J. Appl. Phys.* **69**, 816 (1991).
- [34] R. N. Gurzhi, A. N. Kalinenko, and A. I. Kopeliovich, *Phys. Rev. Lett.* **74**, 3872 (1995).
- [35] K. Damle and S. Sachdev, *Phys. Rev. B* **56**, 8714 (1997).
- [36] H. Buhmann, L. W. Molenkamp, R. N. Gurzhi, A. N. Kalinenko, A. I. Kopeliovich, and A. V. Yanovsky, *Low Temp. Phys.* **24**, 737 (1998).
- [37] H. Predel, H. Buhmann, L. W. Molenkamp, R. N. Gurzhi, A. N. Kalinenko, A. I. Kopeliovich, and A. V. Yanovsky, *Phys. Rev. B* **62**, 2057 (2000).
- [38] A. V. Andreev, S. A. Kivelson, and B. Spivak, *Phys. Rev. Lett.* **106**, 256804 (2011).
- [39] D. Forcella, J. Zaanen, D. Valentinis, and D. van der Marel, *Phys. Rev. B* **90**, 035143 (2014).
- [40] A. Tomadin, G. Vignale, and M. Polini, *Phys. Rev. Lett.* **113**, 235901 (2014).
- [41] P. S. Alekseev, *Phys. Rev. Lett.* **117**, 166601 (2016).
- [42] A. B. Kashuba, *Phys. Rev. B* **78**, 085415 (2008).
- [43] L. Fritz, J. Schmalian, M. Müller, and S. Sachdev, *Phys. Rev. B* **78**, 085416 (2008).
- [44] M. Müller, J. Schmalian, and L. Fritz, *Phys. Rev. Lett.* **103**, 025301 (2009).
- [45] M. Mendoza, H. J. Herrmann, and S. Succi, *Phys. Rev. Lett.* **106**, 156601 (2011).
- [46] B. N. Narozhny, I. V. Gornyi, M. Titov, M. Schütt, and A. D. Mirlin, *Phys. Rev. B* **91**, 035414 (2015).
- [47] A. Cortijo, Y. Ferreirós, K. Landsteiner, and M. A. H. Vozmediano, *Phys. Rev. Lett.* **115**, 177202 (2015).
- [48] L. Levitov and G. Falkovich, *Nat. Phys.* **12**, 672 (2016).
- [49] G. Falkovich and L. Levitov, *Phys. Rev. Lett.* **119**, 066601 (2017).
- [50] S. Danz and B. N. Narozhny, *2D Materials* **7**, 035001 (2020).
- [51] H.-Y. Xie and A. Levchenko, *Phys. Rev. B* **99**, 045434 (2019).
- [52] S. Danz, M. Titov, and B. N. Narozhny, [arXiv:1912.12341](https://arxiv.org/abs/1912.12341).
- [53] We assume for simplicity that the embedding matrix and substrate have the same dielectric constant  $\epsilon$ .
- [54] This equation interpolates between asymptotes at  $r \gg a$ , where one can put  $a = 0$  and the case  $r \ll 1/|k|$ , where one can use expansion over  $k$  up to first order with the parametrical matching at  $a \ll r \ll 1/|k|$ .
- [55] E. Borovitskaya, W. Knap, M. S. Shur, R. Gaska, E. Frayssinet, P. Lorenzini, N. Grandjean, B. Baumont, J. Massies, C. Skierbiszewski, P. Prystawko, M. Leszczynski, I. Grzegory, and S. Porowski, *MRS Proceedings* **639**, G7.5 (2000).
- [56] R. Gaska, M. S. Shur, A. D. Bykhovski, A. O. Orlov, and G. L. Snider, *Appl. Phys. Lett.* **74**, 287 (1999).
- [57] I. Akimoto, Y. Handa, K. Fukai, and N. Naka, *Appl. Phys. Lett.* **105**, 032102 (2014).
- [58] N. Naka, K. Fukai, Y. Handa, and I. Akimoto, *Phys. Rev. B* **88**, 035205 (2013).
- [59] Pietro P. Altermatt, Andreas Schenk, Frank Geelhaar Gernot Heiser, *J. Appl. Phys.* **93**, 1598 (2003).
- [60] <http://www.semiconductors.co.uk/propiviv5431.htm>.
- [61] Yu. A. Goldberg and N. M. Schmidt, *Handbook Series on Semiconductor Parameters*, Vol. 2, edited by M. Levinshtein, S. Rumyantsev and M. Shur (World Scientific, London, 1999), pp. 62-88.
- [62] M. E. Levinshtein, S. Rumyantsev, and M. S. Shur (Eds.), *Handbook of Semiconductor Material Parameters, Si, Ge, C (diamond), GaAs, GaP, GaSb, InAs, InP, InSb*, Vol. 1 (World Scientific, Singapore, 1996).
- [63] R. J. Nicholas, J. C. Portal, C. Houlbert, P. Perrier, and T. P. Pearsall, *Appl. Phys. Lett.* **34**, 492 (1979).
- [64] W. Knap, V. I. Fal'ko, E. Frayssinet, P. Lorenzini, N. Grandjean, D. Maude, G. Karczewski, B. L. Brandt, J. Lusakowski, I. Grzegory, M. Leszczynski, P. Prystawko, C. Skierbiszewski, S. Porowski, X. Hu, G. Simin, M. A. Khan, and M. S. Shur, *J. Phys.: Condens. Matter* **16**, 3421 (2004).